BULLETIN OF THE EARTHQUAKE
RESEARCH INSTITUTE
Vol. 58 (1983), pp. 591-646

24. *Spatial Variation of Earthquake-Generating Stress in and around the Kanto District, Central Japan.**

By Tadashi MAKI,

Earthquake Research Institute, University of Tokyo.

(Received July 30, 1983)

Abstract

A number of fault-plane solutions of earthquakes (n=454) in and around the Kanto District were determined by a numerical method, and the spatial variation of earthquake-generating stress is derived by using individual and average focal mechanisms. Averaging of direction cosines is made for both axes of maximum pressure and tension, and other axes are located by computation. The structure of earthquake-generating stress is derived from the spatial variation of fault types which are systematically classified into six types based on dip angles and azimuths of pressure and tension axes and null vector. The spatial variations of focal mechanisms are derived by summarizing pressure and tension axes and comparing them with the distribution of earthquake hypocenters previously determined by correcting the Pn station biases. The northern focal hemispheres of fault-plane solutions are used for comparison with the vertical distributions of the relocated hypocenters.

A reverse fault with the horizontal E-W compression is predominant for crustal and subcrustal earthquakes on the Pacific side, and it is directly related to the westward convergence of the Pacific Plate underneath the Eurasian Plate. Axes of maximum pressure show some variations for individual earthquakes and hypocenter locations. An eastward increase of dip angle of T axis is observed along the E-W section. The E-W compression appears also in the inland region of the northern Kanto District. In the southwestern part of the Kanto District a variety of focal mechanisms are observed. For very shallow earthquakes near Izu-Oshima and the Izu Peninsula a strike-slip with an N-S compression is predominant. Another type is the normal faulting for earthquakes located south off the Kanto District. These two types of faulting commonly have the horizontal E-W extension. Besides the down-dip compression observed for mantle earthquakes, the down-dip extension along the inclined seismic zone is observed for intermediate-depth earthquakes located on the Pacific side. But the tensional stresses along the lower plane of the double seismic zone show a variety of azimuths and dip angles.

* Read on December 21, 1982, at the monthly meeting (Danwakai) of the Earthquake Research Institute.

A significant contrast is observed in fault types between the Izu-Bonin region and the Pacific coast of the Kanto District and Northeast Japan. The thrust faulting is predominant for earthquakes with depths down to 60 km along the plate boundary below the Pacific coast, but in the Izu-Bonin region various types of faulting are observed without showing an obvious inclined seismic zone. Some source regions with similar focal mechanisms are observed; the reverse fault with the NW-SE compression in the sequence of the 1964 Niigata and 1972 Hachijojima Earthquakes, and the strike-slips in the Matsushiro Swarm and in the Izu Peninsula and Izu Islands region.

1. Introduction

Complexities in the seismic activities and tectonics in and around the Kanto District are considered to be generated by the convengence of three lithospheric plates—the Pacific, the Eurasian and the Philippine Sea Plates (Fig. 1). Some intense clusters of earthquake hypocenters and systematic variation of focal mechanisms are noticeable features especially in the Kanto District (MAKI *et al.*, 1980). Recently it become possible to obtain a large number of fault-plane solutions of earthquakes in and around the Kanto District by a new numerical method (MAKI, 1982). In the present study the spatial variation of focal mechanisms will be studied in more detail from these fault-plane solutions. The location and size of source regions with regular focal mechanisms will be also derived. The fine structure of earthquake-generating stress will be studied by comparing with the precise hypocenter locations which are determined by correcting the station biases of Pn travel time (MAKI, 1981a).

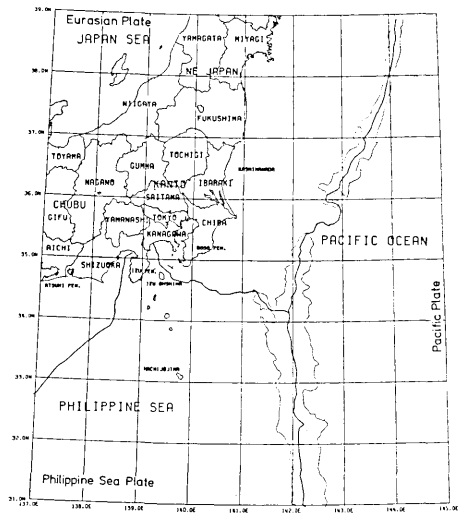

Fig. 1. Location map of the Kanto District and its vicinity. The Japan Trench is outlined by the bathymetric contour lines of 7000 m. Boundaries of the plates are denoted by the trench or trough axes of thick lines.

The tectonic stress cannot be directly estimated only from fault-plane solutions of individual earthquakes, but spatial regularities of focal mechanism may be useful in elucidating the state of tectonic stress. In the previous

studies the regularities of focal mechanisms have been estimated by summarizing the fault-plane solutions or by detecting systematic trends in the geographical distribution of focal mechanisms. Averaging of fault-phase solutions has been made by SCHEIDEGGER (1958) and RITSEMA and SCHOLTE (1961) to obtain the mean axis of null vectors from nodal planes. FARA and SCHEIDEGGER (1963) revised the analytical method by finding the eigenvector in the least-squares method. ICHIKAWA (1970a, b) compared the spatial variation of mean directions of only the pressure axes of earthquakes in and near the Izu Peninsula. Complete sets of average fault-plane solutions have not been included in these studies. In this paper the average fault-plane solutions will be given for earthquakes selected for source regions. At first the average axes will be obtained for maximum pressure and tension, and then the null vector and poles of nodal planes will be located by computation.

Catalogues of fault-plane solutions have been published by FARA (1964) and WICKENS and HODGSON (1967) for earthquakes in the world, and by ICHIKAWA (1971, 1979) and YOSHII (1979a) for earthquakes in and around the Japanese Islands. The number of earthquakes in these catalogues is not sufficient for studies of the tectonic stress in specific regions. Fault-plane solutions of earthquakes in the Kanto District have been studied by ICHIKAWA (1962, 1970a, b), MAKI (1974) and MAKI *et al.* (1980). In the present study fault-plane solutions will be determined systematically for all the earthquakes occurred in and around the Kanto District.

Recently focal mechanisms were studied in terms of the spatial distribution in several areas in the world; by CARDWELL and ISACKS (1978) for the Banda Sea, by FORSYTH (1975) for the South Atlantic and Scotia Sea, by PASCAL *et al.* (1978) for the New Hebrides Arc, by STAUDER (1973) for Chile, by STAUDER (1975) for Peru, by STEIN *et al.* (1982) for the Lesser Antilles Arc, by VEITH (1974, 1977) and STAUDER and MUALCHIN (1976) for the Kurile Arc, and by AOKI (1974), SHIONO and MIKUMO (1975), UMINO and HASEGAWA (1975, 1982), SASATANI (1976), SHIONO (1977), HASEGAWA *et al.* (1978a, b), MAKI *et al.* (1980), SHIONO *et al.* (1980) and UKAWA (1982) for the Japan arcs. Global surveys of focal mechanisms were made by ISACKS and MOLNAR (1971), ISACKS and BARAZANGI (1977) and FUJITA and KANAMORI (1981). In the present study the structure of earthquake-generating stress in and around the Kanto District will be derived in more detail from the spatial variation of focal mechanisms in the Kanto District and vicinity.

Some intense clusters of earthquake hypocenters in the Kanto District have been shown by TSUMURA (1973), USAMI and WATANABE (1975), MAKI *et al.* (1980), MAKI and TSUMURA (1980) and MAKI (1981b)

from small- and micro-earthquakes observed by the high-sensitivity seismographs. These features were also identified by the precisely relocated hypocenters of larger earthquakes (MAKI and TSUMURA, 1980; MAKI, 1981a, b). Focal mechanisms may be useful for understanding the causes of such intense clusters of hypocenters. There is a distinct boundary of longitude 139°E in the spatial variation of focal mechanisms of shallow earthquakes near the Izu Peninsula, namely the horizontal N-S compression of the strike-slip on the western side and the NW-SE compression on the eastern side (ICHIKAWA, 1962, 1970a, b; MAKI, 1974; SOMERVILLE, 1978; NAKAMURA, 1979). Two types of focal mechanisms of the low-angle thrust and vertical slip with the western side downgoing were observed for earthquakes in the southwestern part of the Ibaraki Prefecture by MAKI *et al.* (1980) and MAKI (1981b). Earthquakes below the middle part of the Chiba Prefecture were interpreted by the vertical slip along the N-S striking plane (MAKI *et al.*, 1980; SOMERVILLE, 1980).

Depth distributions of micro-earthquakes at depths from 80 to 200 km show a double-planed seismic zone in the Kanto District (TSUMURA, 1973) and in Northeast Japan (HASEGAWA *et al.*, 1978a, b). A detailed cross section of the deep seismic zone in Northeast Japan was shown by YOSHII (1979). He obtained a very thin seismic zone accompanied by another seismic plane 30 km below by using focal depth estimated by pP-P times, and showed the systematic variation of focal mechanisms along the seismic zone, namely the normal fault near the trench wall, the low-angle thrust along the deep seismic zone and the horizontal E-W compression of shallow earthquakes in the inland region. A down-dip compression is predominant for earthquakes along the upper plane of the double seismic zone, and a down-dip extension for the lower plane. In this paper spatial variation of focal mechanisms in the Kanto District will be presented in more detail with relation to the double seismic zone.

2. Fault-plane solutions by the new numerical method

Fault-plane solutions of earthquakes ($M \geqq 5.0$) in and around the Kanto District have been determined by a new numerical method (MAKI, 1982). In this method fault-plane solutions with plausible scores of consistent first-motion data are adopted from 6156 tentative sets of maximum pressure and tension axes located at the 10° interval of dip angles and azimuths. First-motion data with lower consistencies are discarded by an objective and automatic way. Fault-plane solutions with scores of 95% or more are used to represent confidence regions of fault-plane solutions. Null vector and poles of nodal planes are

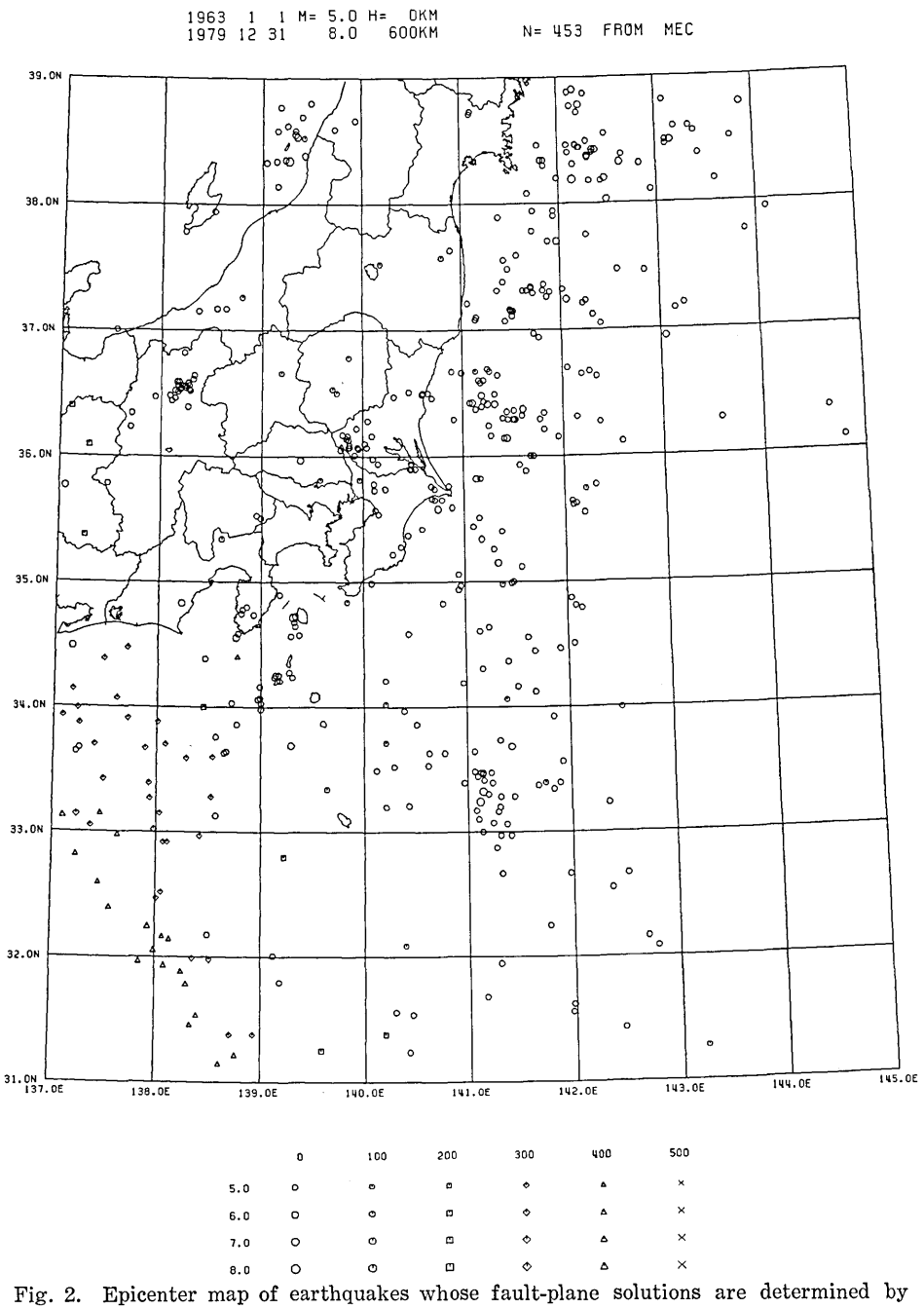

Fig. 2. Epicenter map of earthquakes whose fault-plane solutions are determined by the numerical method. The earthquakes are limited to those which occurred in and around the Kanto District during the period of 17 years from 1963 to 1979, with earthquake magnitudes of 5.0 or more. Focal depths and earthquake magnitudes are indicated by classified symbols shown in the legend.

located by computation from possible sets of P and T axes.

The numerical method was applied to 459 earthquakes with magnitude of 5.0 or more, which occurred during the period of 17 years from 1963 to 1979 in the region bounded by latitudes 31°N and 39°N and longitudes 137°E and 145°E. Usable fault-plane solutions with scores of 95% or more could be obtained for 454 earthquakes, whose epicenters are shown in Fig. 2. Focal depths are shown by different symbols for every 100 km and the symbols are classified according to earthquake magnitudes, as shown in the legend of the figure. No usable solutions were obtained for the remaining five earthquakes due to scores less than 95%.

In the Appendix equal-area projections of fault-plane solutions are shown for only a few earthquakes, which are mentioned in the text, to save space. Fault-plane solutions with scores of 99% or more are indicated by asterisks ("*"), and for solutions with scores from 95% to 98% by letters "P", "T" and "N" on the left-hand side. These solutions with scores over 95% constitute confidence regions of fault-plane solutions. The most probable solution of focal mechanism and first-motion data are shown on the right-hand side. Open and solid circles show dilatation and compression of first-motion data, and "A" and "B" denote poles of nodal planes, respectively. Dip directions and dip angles of maximum pressure and tension, null vector and poles of nodal planes are given at the bottom of each figure. Origin times and focal coordinates are given at the top. Origin times and hypocenter locations were determined by correcting the station biases of Pn travel time (MAKI, 1981a). For earthquakes whose fault-plane solutions cannot be determined with scores of 95% or more in the first run, tenth digits of greatset score are shown as seen by "7", "8" for earthquakes on Apr. 22, 1966, Mar. 19, 1967 and Sep. 15, 1971 in the Appendix. More possible fault-plane solutions could be obtained after discarding apparently inconsistent first-motion data.

Fault-plane solutions were previously determined for some larger earthquakes by using first-motion data read on the WWSSN seismogram for the Niigata Earthquake on June 16, 1964 (HIRASAWA, 1965; ABE, 1975a), the Kashimanada Earthquake on Sep. 18, 1965 (SASATANI, 1971; MAKI, 1975a), the East Saitama Earthquake on July 1, 1968 (ABE, 1975a), the Middle Gifu Earthquake on Sep. 9, 1969 (MIKUNO, 1973), the Hachijojima Earthquake on Dec. 4, 1972 (MAKI, 1975b), the Off Izu Peninsula Earthquake on May 9, 1974 (MAKI, 1974; ANDO and MIKUNO, 1974; MATSUZAKI and KAWASAKI, 1974; ABE, 1978), the Near Izu-Oshima Earthquake on Jan. 14, 1978 (SHIMAZAKI and SOMERVILLE, 1978, 1979) and the Off Miyagi Prefecture Earthquake on

June 12, 1978 (SENO *et al.*, 1980). These solutions seem to be identical comparing with the confidence regions of faut-plane solutions in the present study.

For earthquakes that occurred in and around the Kanto District with magnitudes of 5.0 or more, the number of earthquakes in the Ichikawa and JMA catalogues of fault-plane solutions is only 58% of of the number in the present study. A complete selection of earthquakes with magnitudes over a certain level was not made in these catalogues. Fault-plane solutions of some large earthquakes were not given in those catalogues. For some earthquakes faut-plane solutions were determined by less numbers of first-motion data than in the present study.

Table 1. Examples of relative angular distances (in degrees) between the poles of nodal planes, axes of null vector and maximum pressure and tension. Azimuths of dip directions ("dd") are measured clockwise from the north and dip angles ("d") from the horizon. Cases where the orthogonal relation does not hold due to greater or smaller distance by 0.3° are marked by "*".

(1)

Date y m d	Or. time h m s	Lat °N	Long °E	Dep km	Mag	Obs NR	Obs NU
63 8 18	16 9 49	35.81	139.58	154.7	5.3	34	27

Pole-X		Pole-Y		Null axis		P-axis		T-axis	
dd	d	dd	d	dd	d	dd	d	dd	d
192.3	69.7	79.1	8.4	346.5	18.8	100.0	50.0	243.0	33.8
0.000		89.897		89.624*		44.805		45.223	
		0.020		89.737		45.093		44.882	
				0.020		89.757		90.250	
						0.034		90.025	
								0.048	

(2)

Date y m d	Or. time h m s	Lat °N	Long °E	Dep km	Mag	Obs NR	Obs NU
64 6 16	13 58 46	38.69	139.40	34.1	5.1	11	10

Pole-X		Pole-Y		Null axis		P-axis		T-axis	
dd	d	dd	d	dd	d	dd	d	dd	d
95.6	12.8	329.5	68.5	189.3	17.2	290.0	30.0	74.0	54.5
0.000		90.255		89.691*		44.993		45.019	
		0.034		89.648*		44.755		45.237	
				0.028		90.329*		89.790	
						0.028		89.989	
								0.028	

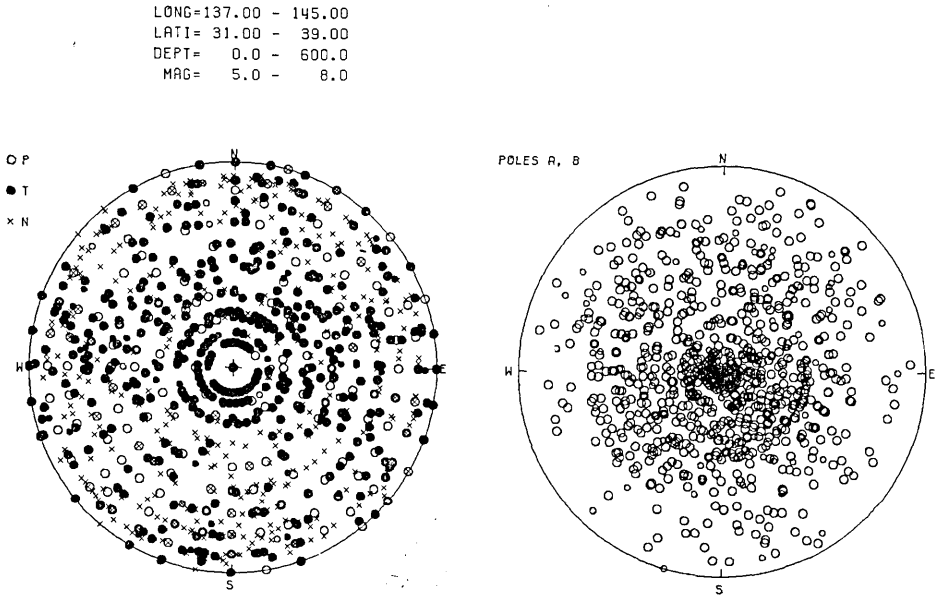

Fig. 3. Summary of 524 fault-plane solutions for 454 earthquakes which occurred in and around the Kanto District during the period from 1963 to 1979 with magnitudes of 5.0 or more. Axes of maximum pressure (P), tension (T) and null vector (N) are represented by open and solid circles and crosses on the left, and poles of nodal planes by open circles on the right.

The orthogonal relation in the fault-plane solutions obtained in the present study has been examined. In Table 1 the relative angular distances between the stress axes and poles of nodal planes are shown for two earthquakes. According to the definition of fault-plane solution in the source model of double couple, the angular separation between the stress axes (P, T and N) and between the poles of nodal planes should be 90°. Angular separation between the compression and tension axes (P and T) and poles of nodal planes (A and B) should be 45° or 135°. In all the 524 solutions for 454 earthquakes including multiple solutions, the orthogonal relation are held within differences of angular distances less than 0.4°. Absolute differences of 0.3° or more compared with the orthogonal relation are marked by asterisks (*) in the table. In order to keep the orthogonal relation within 1°, it is necessary to give figures in fault-plane solutions by the unit of tenths of a degree.

In Fig. 3 fault-plane solutions are summarized for all the earthquakes. On the left-hand side the axes of maximum pressure ("P"), tension ("T") and null vector ("N") are shown by open and solid circles and crosses, respectively. On the right-hand side the poles of nodal planes are shown. No systematic trends can be read from these distributions. These fault-plane solutions will be studied with respect

to regional variation of focal mechanisms.

3. Averaging method of fault-plane solutions

Fault-plane solutions of large earthquakes may better represent the tectonic stress in a region. However it is not understood what level of earthquake magnitude can be representative of the tectonic stress. When many fault-plane solutions are obtained, earthquake-generating stress may be found by averaging solutions. Only a few studies have been made for averging focal mechanisms (SCHEIDEGGER, 1958; RITSEMA and SCHOLTE, 1961; FARA and SCHEIDEGGER, 1963; ICHIKAWA, 1970a, b). In these studies complete sets of axes in fault-plane solutions have not been treated. In the present study a full representation of average fault-plane solutions is treated, especially the combined stress axes of maximum pressure and tension.

Averaging of fault-plane solutions in the present study is made as follows: (1) omitting axes of maximum pressure and tension accompanied by large relative separation from the rest, (2) locating mean axes of maximum pressure and tension by averaging direction cosines, and (3) locating other axes from the mean axes of maximum pressure and tension by computation. Fig. 4 shows the equal-area projection of 45 axes of maximum pressure on the lower focal hemisphere for the intermediate-depth earthquakes with focal depths from 200 to 400 km. Westward plunging axes of maximum pressure are predominant and relatively independent of other axes of maximum pressure located on the eastern side.

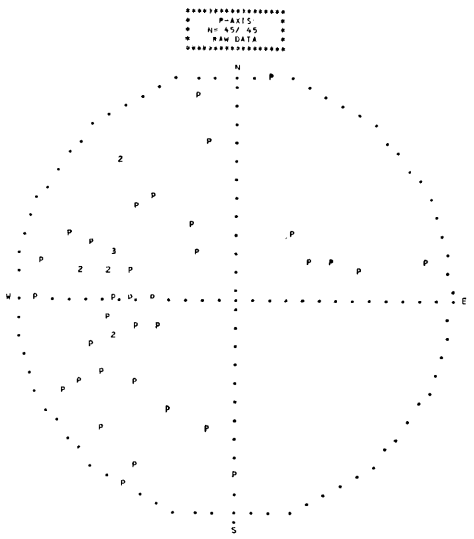

Fig. 4. Equal-area projection of maximum pressure (P) on the lower focal hemisphere for errthquakes with focal depths from 200 to 400 km. Numerals mean numbers of P axes within the same columns.

From the idea of double-couple source model the critical angle is 45° for distinguishing near or distant solutions from others on the focal sphere. Axes with relative angular distances over 135° are rather near to opposite axes of the force couples. Thus relative angular distances are classified into three

ranges as "near distances" from 0° to 45°, "far distances" from 45° to 135°, and "near but opposite distances" from 135° to 180°. Relative angular distances are calculated for individual axes, and axes accompanied over half by far distances may be omitted.

Mean locations of P and T axes are obtained by the arithmetic averaging of direction cosines. Comparing frequencies for 0.1-increment of direction consines, axes located far from the peak frequency are again omitted. Mean values of direction cosines are normalized using any value of v as

$$\left(\frac{\bar{a}_x}{v}\right)^2+\left(\frac{\bar{a}_y}{v}\right)^2+\left(\frac{\bar{a}_z}{v}\right)^2=1\ ,$$

were $\bar{a}_w$, $\bar{a}_y$ and $\bar{a}_z$ denote mean direction cosine to the x, y and z coordinates. Average locations of the maximum pressure and tension are independently determined by the above method, and then the orthogonal relation between these P and T axes may not be strictly held as 90°.

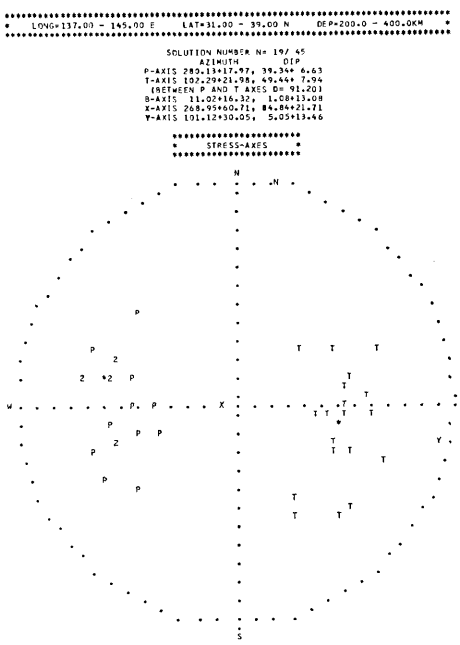

Fig. 5. Average fault-plane solutions for earthquakes with focal depths from 200 to 400 km. "P" and "T" denote useful solutions, and asterisks ("*") denote the average locations of P and T axes, respectively. Poles of nodal planes and axes of null vector obtained by computation from the average P and T axes are shown by "X", "Y" and "N".

Fig. 5 denotes an average fault-plane solution for the intermediate-depth earthquakes. The average P and T axes are denoted by asterisks (*), and "P" and "T" mean usable axes of the maximum pressure and tension (19 out of 45 solutions). "N", "X" and "Y" denote the null vector, poles of nodal planes obtained from P and T axes by computation. This method is effective for clustering solutions of P and T axes. Scattered solutions may be omitted by a preliminary selection, and several average solutions may be obtained individually for some

groups of fault-plane solutions.

4. Spatial variation of fault-plane solutions

The fault-plane solutions of earthquakes in and around the Kanto District are widely variable as shown in Fig. 3. In this chapter some systematic trends in the spatial variation are derived from the individual and average fault-plane solutions. The stress of minor earthquakes can be produced in smaller source regions, but larger earthquakes must be generated by the tectonic stress over a wide region. The intense clustering of earthquake hypocenters beneath the crust in the Kanto District may not be interpreted simply by the Pacific Plate descending to the west. Another possibility is the stress concentration by the head-on collision of the Pacific Plate with the Philippine Sea Plate (MAKI *et al.*, 1980; MAKI, 1981b). Fault-plane solutions of many earthquakes may be helpful in understanding the mechanisms of such earthquake occurrences.

In Fig. 6 fault-plane solutions are summarized on the equal-area projection of the lower focal hemisphere for shallow earthquakes with depths of $h=0-40$ km ($n=224$) and subcrustal earthquakes with depths of $h=40-100$ km ($n=205$). Axes of maximum pressure and tension and null vector are shown on the left-hand side and poles of nodal planes on the right-hand side. No systematic trends or differences in the fault-plane solutions can be found between these ranges of focal depth. Nearly vertical axes of maximum tension (solid circles) are commonly predominant at these depths.

For crustal and subcrustal earthquakes ($h=0-100$ km) with magnitudes of 6.0 or more, the geographical distribution of focal mechanisms is shown in Fig. 7 by using schematic diagrams. Shaded areas denote dilatational areas of first motion, and open areas denote compressional areas. Axes of maximum pressure and tension and null vector are denoted by "P", "T" and "N" beside the encircled crosses. For some earthquakes with multiple solutions, only the more possible solutions are given by referring to neighbouring earthquakes. First-motion data and confidence region of fault-plane solutions are shown in the Appendix for some earthquakes mentioned in the following.

The reverse faulting with the horizontal E-W compression is observed for such earthquakes on the Pacific side of 140°E as the Off Miyagi Prefecture Earthquake (M7.4) on June 12, 1978, the E Off Hachijojima Earthquake on February 29 (M7.1) and December 4 (M7.2), 1972 and the Kashimanada Earthquake (M6.7) on September 18, 1965. The horizontal E-W extension is predominant for earthquakes located

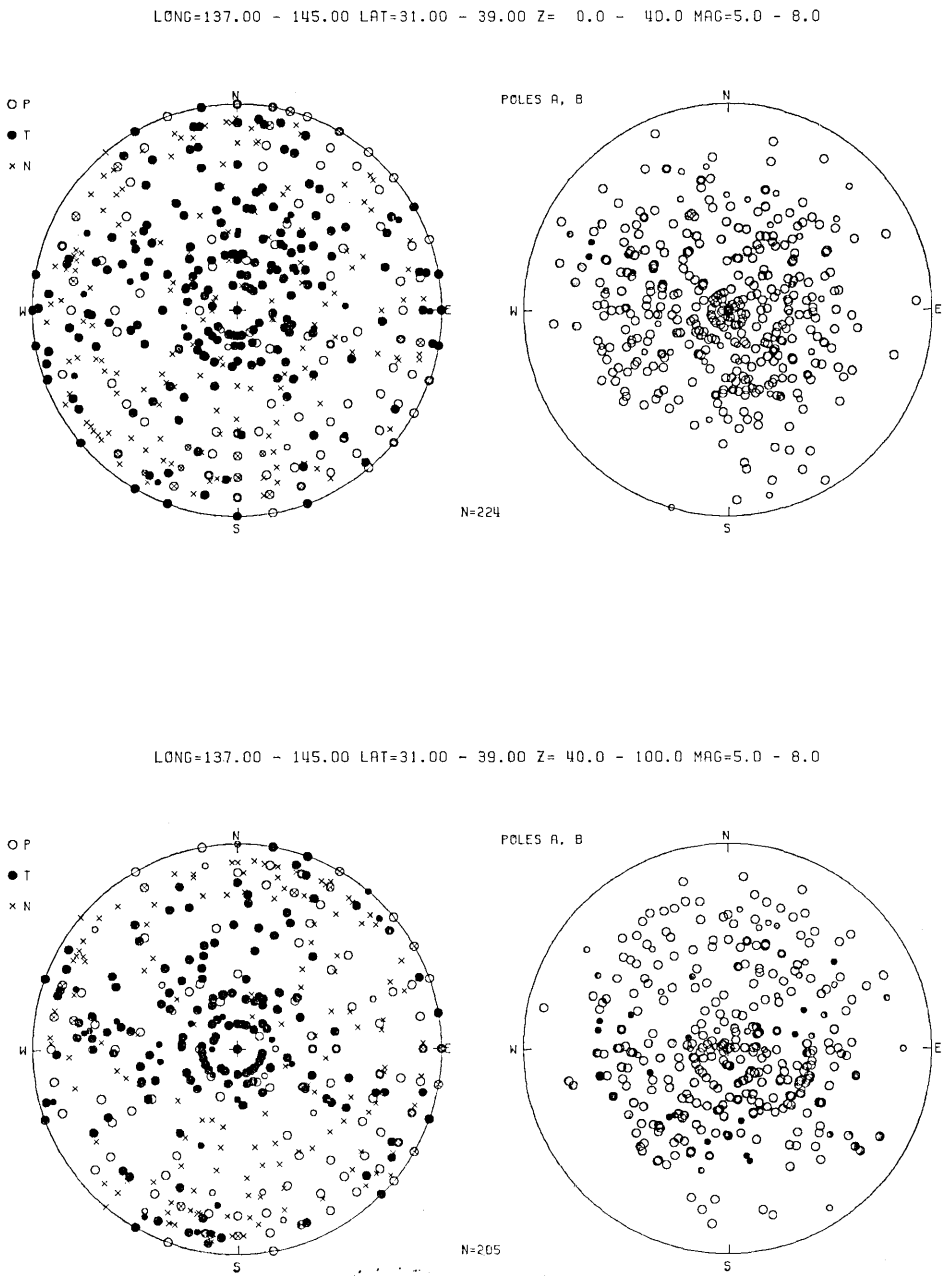

Fig. 6. Summary of fault-plane solutions of crustal earthquakes (h=0−40 km) and subcrustal earthquakes (h=40-100 km) in and around the Kanto District. Symbols are the same as those in Fig. 3.

south off the Kanto District. These earthquakes are divided into two types of focal mechanisms. One is the strike-slip with the N-S compression for the Off Izu Peninsula Earthquake on May 9, 1974 (M6.9)

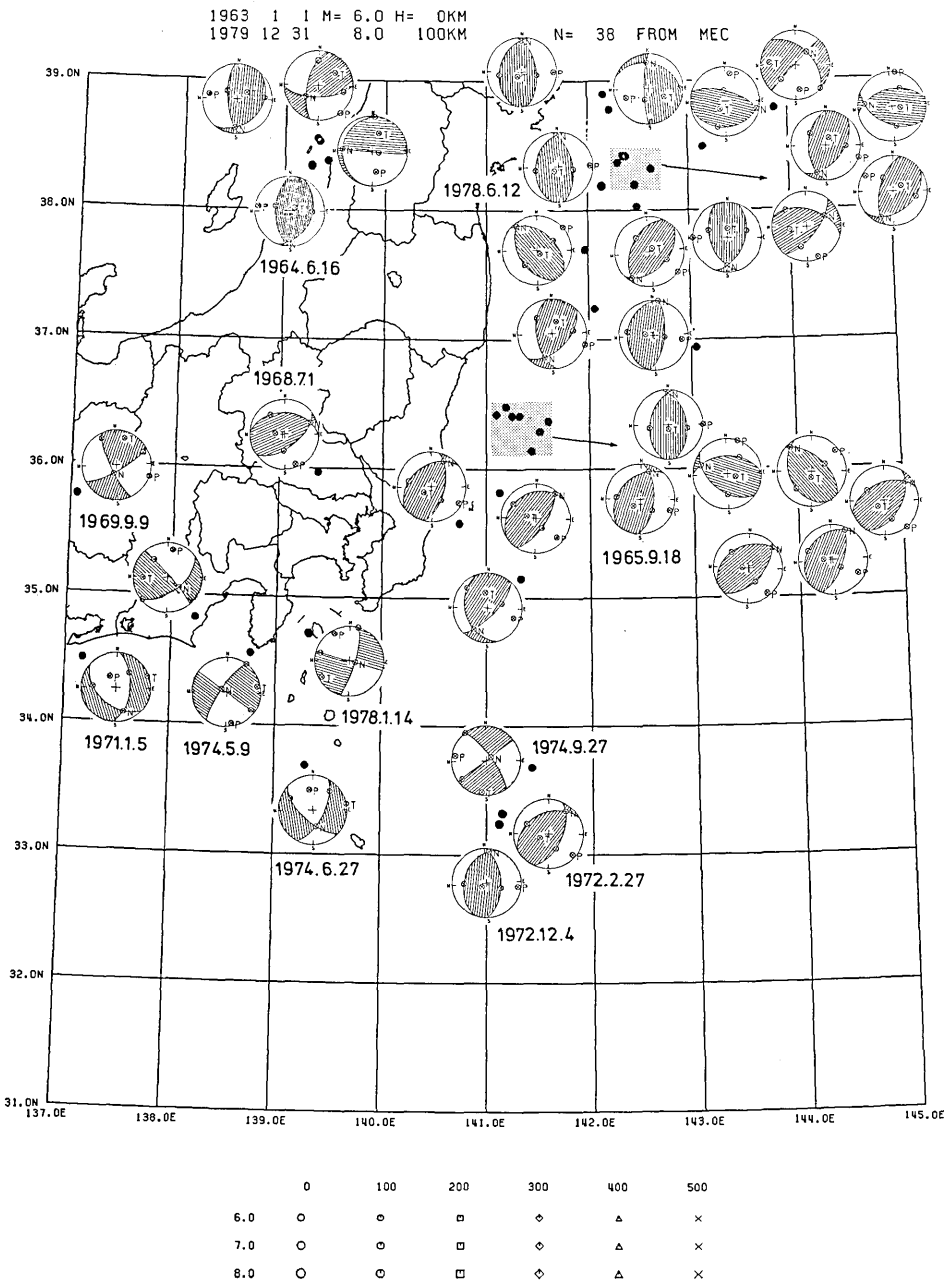

Fig. 7. Schematic diagrams of focal mechanisms for larger earthquakes ($M \geqq 6.0$) in and around the Kanto District. Epicenters are shown by solid circles. Shaded areas denote dilatation of first motion and open areas denote compression. Axes of maximum pressure and tension and null vector are shown by "P", "T" and "N", respectively.

and the Near Izu Oshima Earthquake on January 14, 1978 (M7.0). The other is normal faulting for the earthquake south off Atsumi

Peninsula, Aichi Prefecture, on January 5, 1971 (M6.1) and the one northwest far off Hachijojima Island on June 27, 1974 (M6.1). Earthquakes in the inland region show the strike-slip with the horizontal E-W compression as the Middle Gifu Prefecture Earthquake on September 9, 1969 (M6.6). The Middle Saitama Prefecture Earthquake on July 1, 1968 (M6.1) shows the reverse faulting with the horizontal N-S compression. Widely variable focal mechanisms are observed even for some large earthquakes with magnitudes over 6.0 and suggest a regional variation of tectonic stress.

Spatial variation of fault-plane solutions will be discussed for four ranges of focal depths, namely shallow earthquakes with focal depths from 0 to 40 km, subcrustal earthquakes from 40 to 100 km, and mantle earthquakes with depth ranges of $h=100$-200 km and $h=200$-600 km. Further regional variations are discussed by dividing the Kanto District and vicinity into four parts for crustal and subcrustal earthquakes.

4.1 Crustal earthquakes with depths of $h=0-40$ km

Fig. 8 compares the summaries of fault-plane solutions of the crustal earthquakes ($h=0-40$ km) in all four quarters. Axes of maximum pressure (P) and tension (T) and null vector (N) are shown by open and solid circles and crosses, respectively. The reverse fault of the nearly vertical extension is commonly observed in all four quarters, especially in the northeastern quarter. Two types of strike-slip with the E-W and N-S compression are also observed in the northwestern and southwestern quarters. Predominant types of faulting cannot be obtained for the southeastern quarter due to the less number of fault-plane solutions.

An average fault-plane solution for the all 58 earthquakes that occurred in the northwestern quarter was effective for only 8 solutions. But by dividing into two groups with 19 and 16 solutions, two types of average fault-plane solution are obtained. The first type is such that tension axes are preliminarily selected around azimuth $\phi=0°$ and dip angle $\delta=90°$, showing the reverse fault of the vertical extension. The second type is selected around azimuth of $\phi=10°$ and dip angle $\delta=0°$, showing the strike-slip with the E-W compression and N-S extension. The first type is observed for some aftershocks of the Niigata Earthquake on June 16, 1964 (M7.5), and the second type for earthquakes of the Matsushiro Swarm that occurred from 1965 to 1968. Average fault-plane solutions for shallow earthquakes are illustrated in Fig. 9 by using schematic diagrams of focal mechanism. Average vectors of maximum pressure and tension are denoted by inward and outward arrows. Epicenters are shown by open circles on the background map.

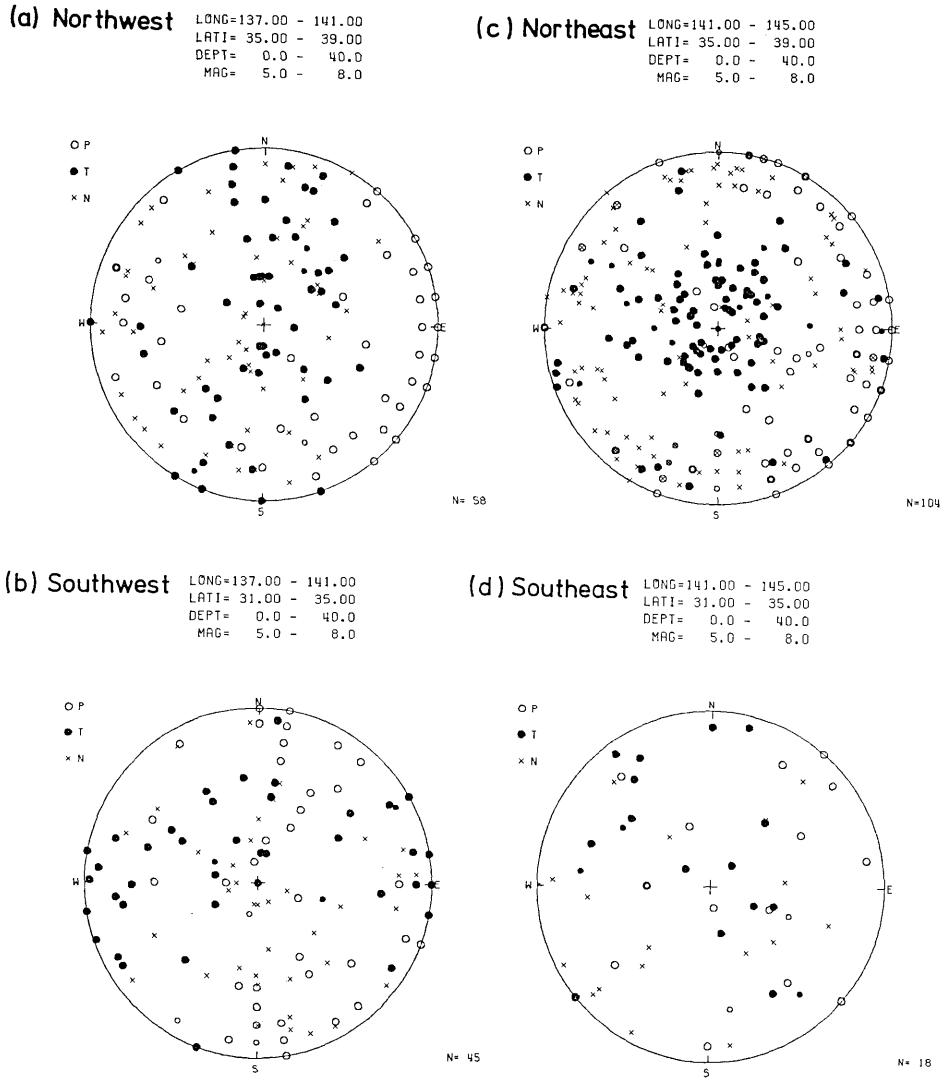

Fig. 8. Regional variation of summarized fault-plane solutions of crustal earthquakes (h=0–40 km) in and around the Kanto District; (a) northwestern, (b) southwestern, (c) northeastern, and (d) southeastern quarters. The Kanto District and vicinity is divided into four parts by the longitude line 140°E and latitude 35°N.

In the southwestern quarter only 12 out of 45 solutions can be interpreted by the strike-slip with the N–S compression and E–W extension. Three types of average focal mechanisms by preliminary selection of tension axes are shown on the lower left-hand side of Fig. 9, the first with T axes around azimuth ϕ=80° and dip angle δ=0°, the second with T axes around azimuth ϕ=330° and dip angle δ=45° and the third with T axes around azimuth ϕ=30° and dip angle

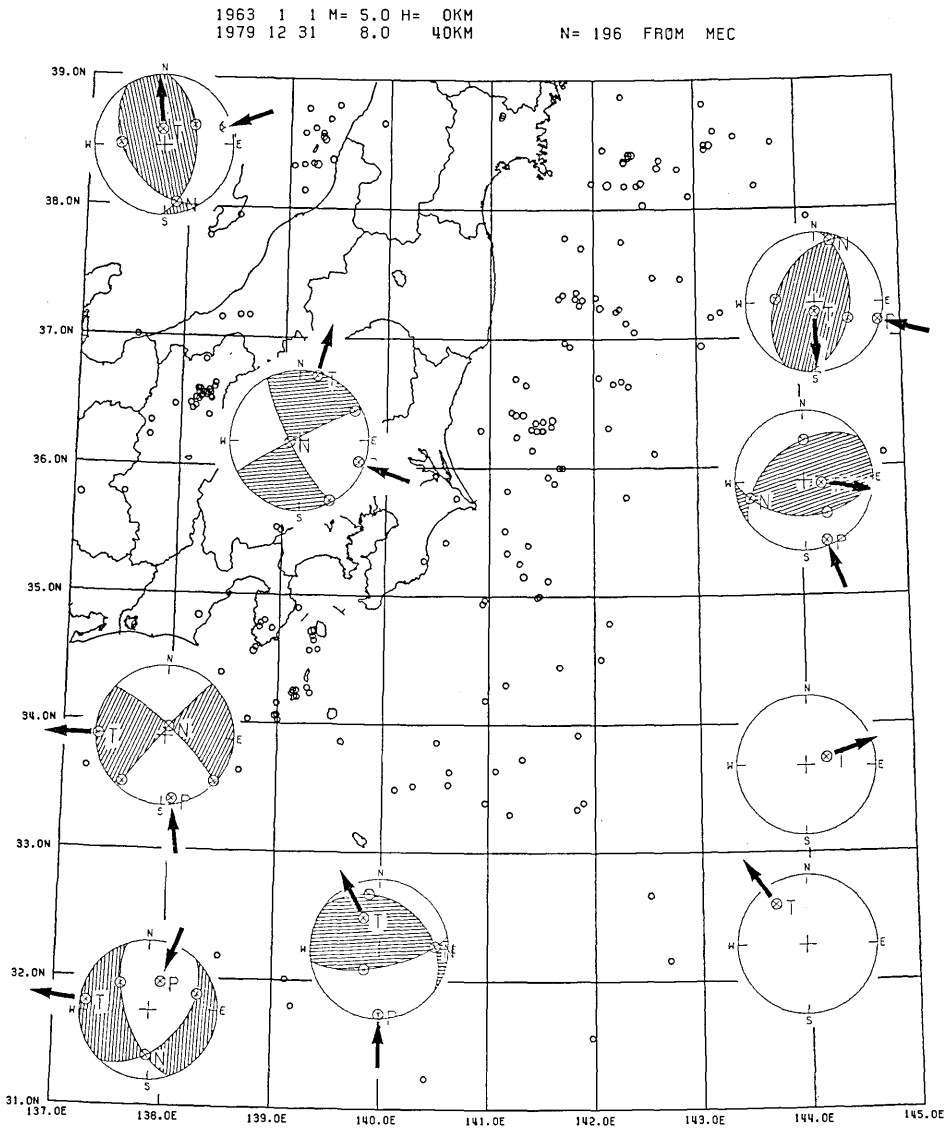

Fig. 9. Regional variation of average fault-plane solutions of crustal earthquakes (h=0–40 km) in and around the Kanto District. Average fault-plane solutions are obtained for earthquakes within every quarter divided by the longitude line 140°E and latitude 35°N, and are represented by schematic diagrams of focal mechanisms. Shaded and open areas denote compression and dilatation of first motion, respectively. Arrows with letters "P" and "T" denote average axes of maximum pressure and tension.

$\delta=60°$. The first type is the strike-slip with the N-S compression and E-W tension, and the second is the reverse fault with the horizontal N-S compression. By the two types of average fault-plane solutions 13 and 9 solutions are interpreted. Nine other solutions show the normal fault with the E-W extension as observed for the earthquakes on January 5, 1971 (M6.1) and June 27, 1974 (M6.1) in Fig. 7.

In the northeastern quarter an average fault-plane solution for 104 solutions is applicable to only three earthquakes. By preliminary classification of solutions with maximum pressure around azimuth $\phi=90°$ and dip angle $\delta=0°$, and azimuth $\phi=10°$ and dip angle $\delta=0°$, two types of average fault-plane solutions of the reverse faults with the horizontal E-W and N-S compression are obtained for 31 and 35 solutions (upper right of Fig. 9). In the southeastern quarter no average solutions were obtained for 18 solutions. Two groups of maximum tension are observed around azimuth $\phi=110°$ and dip angle $\delta=70°$, and azimuth $\phi=310°$ and dip angle $\delta=30°$. These solutions mean the reverse faulting and the NW-SE extension, respectively (lower right of Fig. 9).

4.2 Subcrustal earthquakes with depths of $h=0-100$ km

Fault-plane solutions of subcrustal earthquakes ($h=40-100$ km) are also summarized in Fig. 10. The reverse fault of the vertical extension is predominant all over the region, especially in the northern quarters. But azimuths of maximum pressure are variable, and the horizontal E-W extension is observed for earthquakes in the northeastern quarter and the N-S extension in the southeastern quarter. Fig. 11 shows the geographical distribution of average fault-plane solutions by schematic diagrams. The background map denotes epicenter distribution for this depth range.

In the northwestern quarter 20 out of 53 earthquakes, located in the southwestern part of the Ibaraki Prefecture, are interpreted by the reverse fault with the horizontal E-W compression. Two types of average fault-plane solutions are obtained by preliminary selection, that is the reverse faults with an E-W or N-S compression. In the southwestern quarter two groups of maximum tension are obtained for 19 solutions, showing the horizontal N-S extension and the reverse fault.

For 48 out of 77 solutions in the northeastern quarter an average solution of the reverse fault is obtained for axes of maximum tension around azimuth $\phi=147°$ and dip angle $\delta=80°$. Three types of faulting are obtained by restraining solutions, showing the reverse faults with the horizontal E-W and N-S compression for 27 and 17 solutions, and

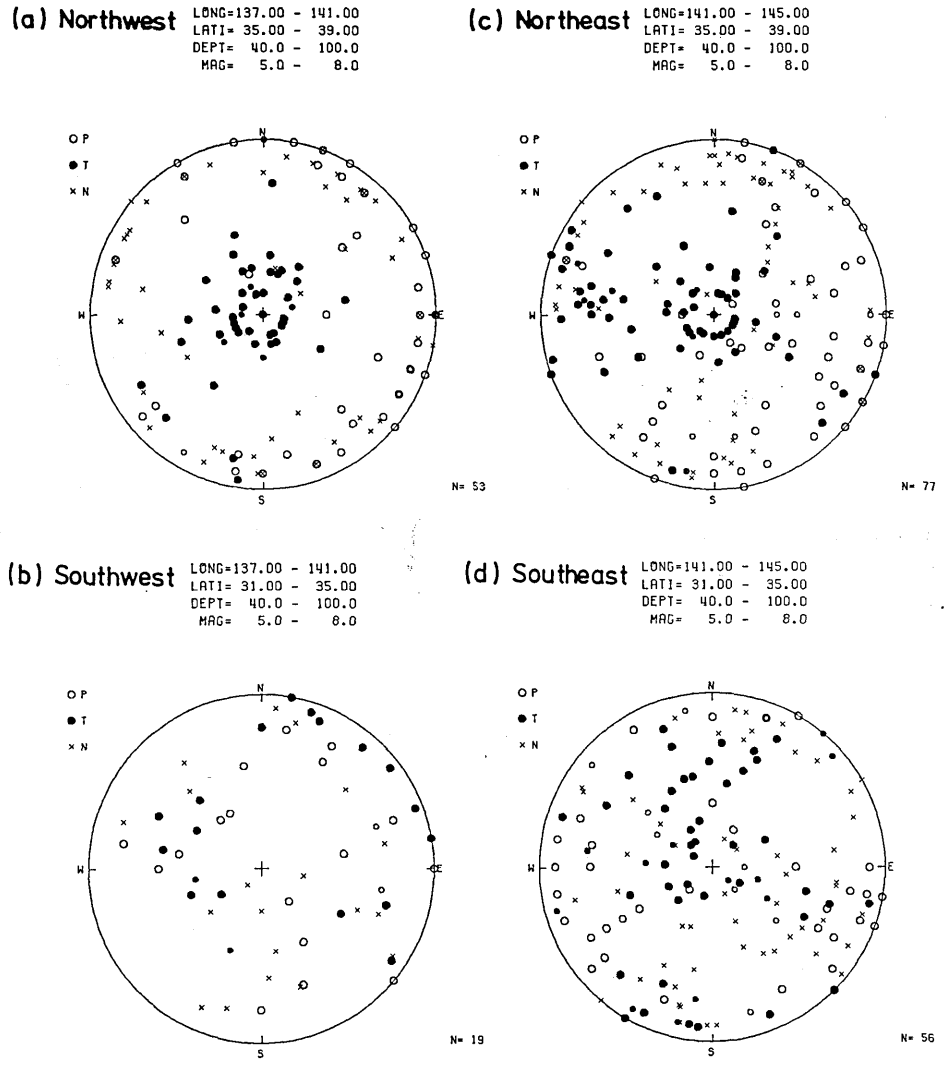

Fig. 10. Regional variation of summarized fault-plane solutions of subcrustal earthquakes (h=40-100 km) in and around the Kanto District; (a) northwestern, (b) southwestern, (c) northeastern, and (d) southeastern quarters.

the normal fault with the horizontal E-W extension for other 8 solutions. In the southeastern quarter average fault-plane solutions are divided into the reverse fault with the horizontal E-W compression and the normal fault with the horizontal N-S extension. The reverse faults are classified into two types of the vertical and northward extension.

4.3 Mantle earthquakes with depths of h=100-600 km

Fault-plane solutions of intermediate-depth earthquakes from 100

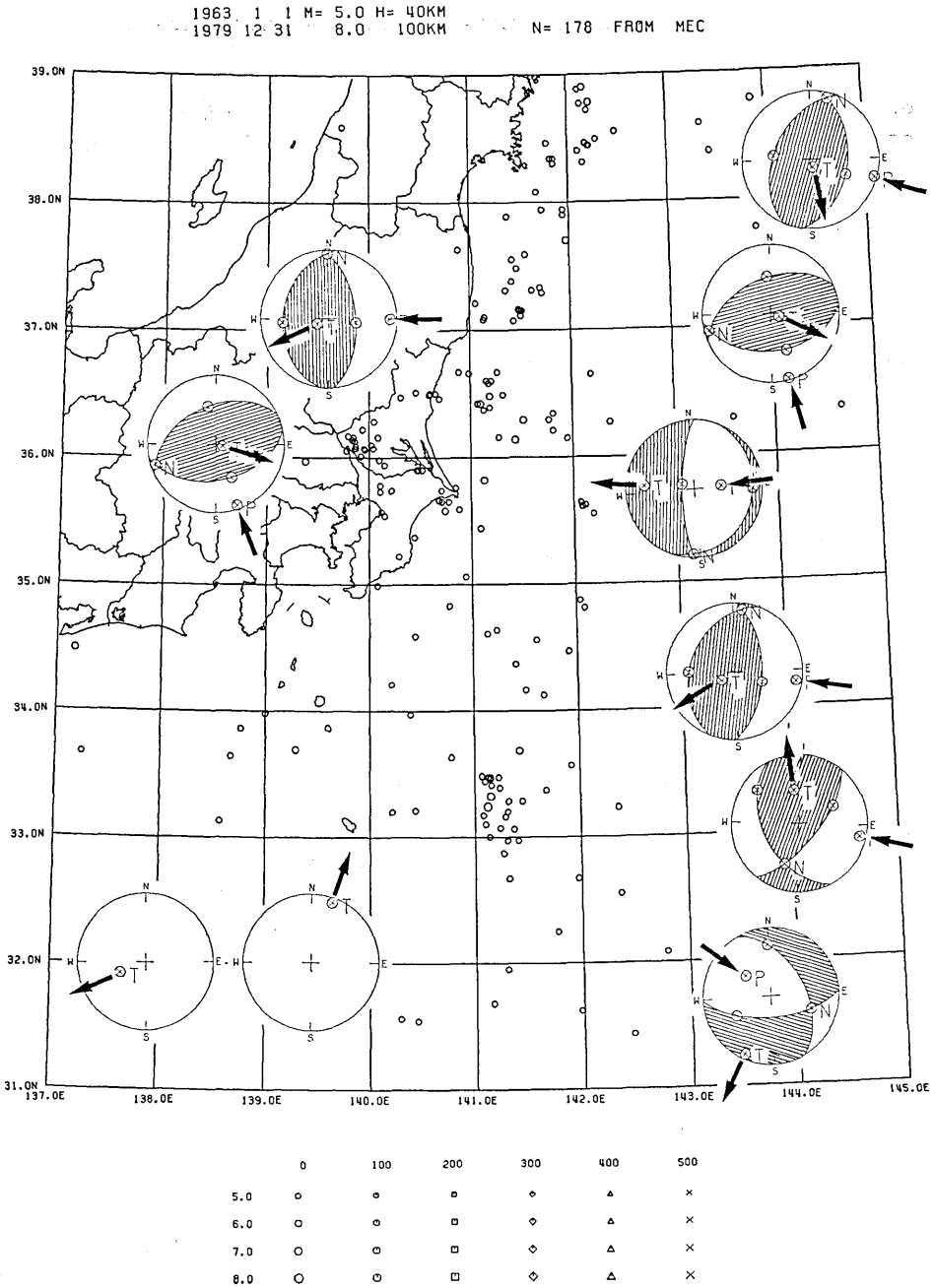

Fig. 11. Regional variation of average fault-plane solutions of subcrustal earthquakes (h=40–100 km) in and around the the Kanto District.

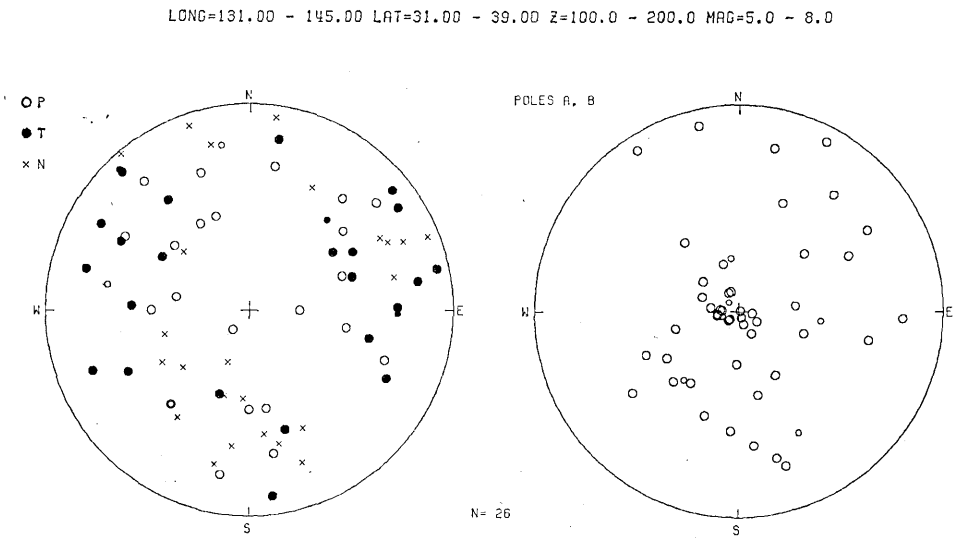

Fig. 12. Summary of fault-plane solutions of mantle earthquakes (h=100–200 km) in and around the Kanto District. Axes of P, T and N are shown by open and solid circles and crosses on the left and poles of nodal planes by open circles on the right.

to 200 km are summarized in Fig. 12. Two groups of maximum tension with eastward and westward plunging are observed. These average fault-plane solutions showing the normal faults with the NW-SE compression and horizontal NW-SE extension are presented by schematic diagrams in Fig. 13. These types show the opposite motions along the inclined seismic zone, namely "down-dip compression" and "down-dip extension" (ISACKS and MOLNAR, 1971). Earthquakes with the down-dip compression are located on the inland side (denoted by "P"), and earthquakes with the down-dip extension on the Pacific side (denoted by "T"). Such a tendancy is consistent with the double seismic zone (HASEGAWA *et al.*, 1978a. b). The third type of faulting is the southward compression. These types of average solutions interpret 7, 8 and 8 solutions, respectively.

Fault-plane solutions of deeper earthquakes from 200 to 600 km are summarized in Fig. 14. Compared to other depth ranges the axes of down-dip compression along the inclined seismic zone are less scattered. An average solution for about half of 67 solutions was obtained as the type of the western side downgoing along the vertical N-S plane with variable azimuths of tension axes from NE to S, shown by schematic diagrams in Fig. 15. Another type of fault with the eastward extension is obtained by preliminary selection of T axes around azimuth ϕ=120° and dip angle δ=30°. Nine other solutions have the southward extension.

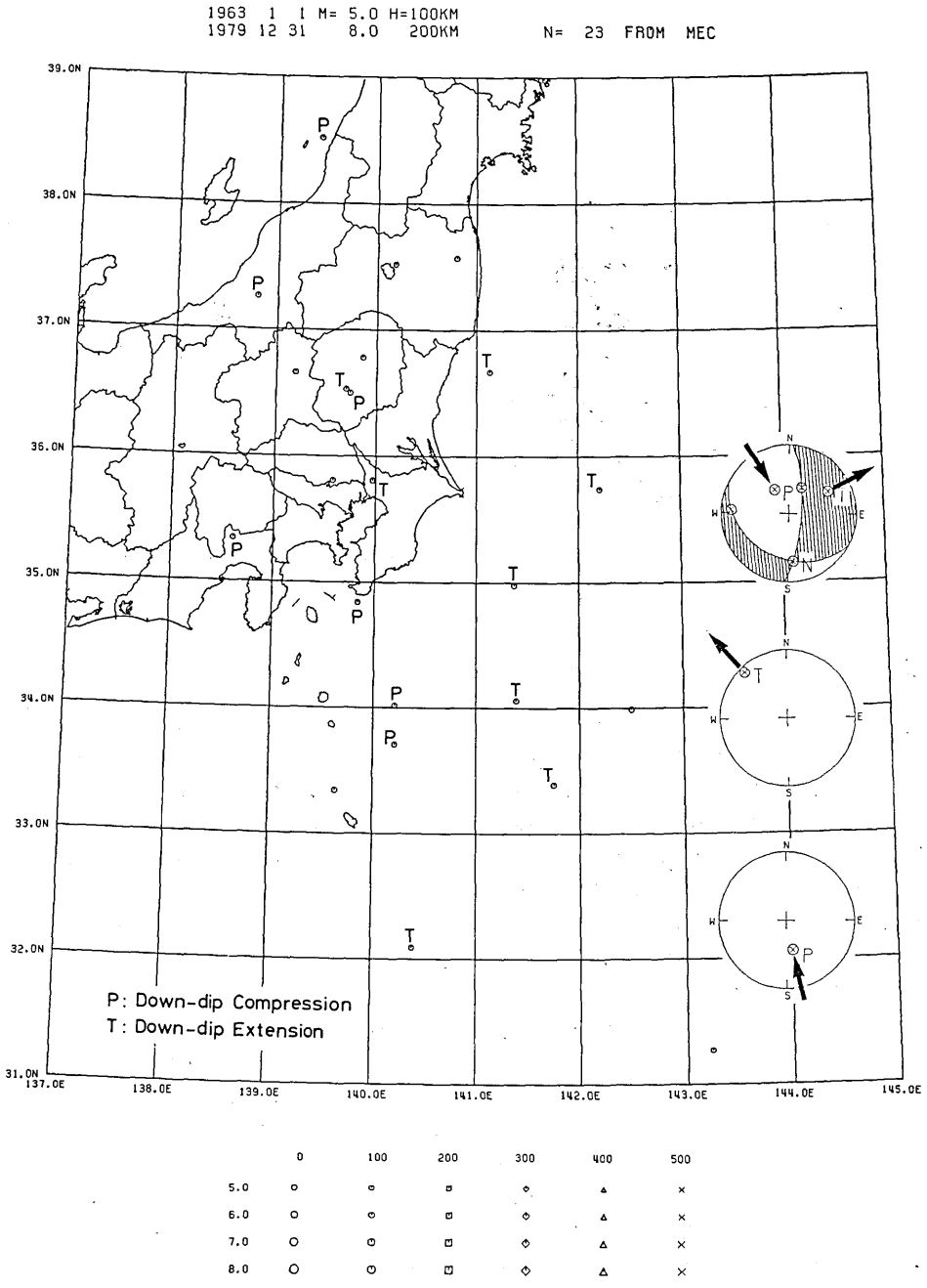

Fig. 13. Regional variation of average fault-plane solutions of mantle earthquakes (h=100–200 km) in and around the Kanto District. Earthquakes of the "down-dip compression" and "down-dip extension" are denoted by "P" and "T" beside the epicenters.

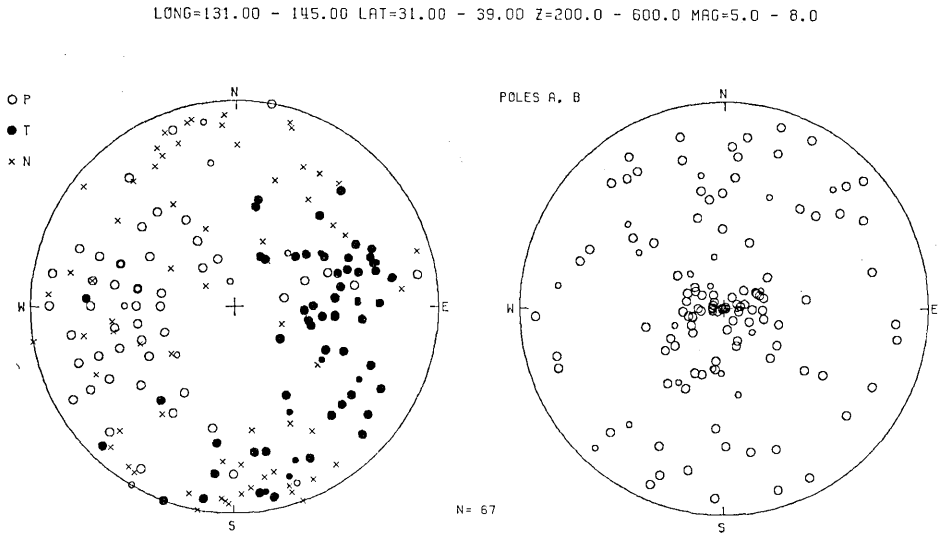

Fig. 14. Summary of fault-plane solutions of deeper mantle earthquakes (h=200-600 km) in and around the Kanto District.

4.4 Average focal mechanisms within 1°-mesh along the E-W section

Summarizing and averaging fault-plane solutions are made for areas of 1°-mesh of latitude and longitude. Average focal mechanisms on the equal-area projection of the northern focal hemisphere are compared with the depth variation of the relocated hypocenters.

Spatial variations of fault-plane solutions along the E-W section of latitude from 38° to 39°N are shown in Fig. 16. Fault-plane solutions are summarized for each 1°-mesh comparing to the focal mechanisms of the Niigata Earthquakes on June 16, 1964 and the off Miyagi Prefecture Earthquake on June 12, 1978 (Fig. 16a). The reverse fault with the E-W compression is predominant in this section. An eastward increase of dip angles of T axes is observed. Fig. 16b shows schematically the equal-area projection of average fault-plane solutions on the lower focal hemisphere for earthquakes within 1°-meshes. The vertical extension is observed for almost all earthquakes, but axes of maximum pressure (P) are variable. Average fault-plane solutions are compared with the depth variation of relocated hypocenters (MAKI, 1981a) by using the equal-area projection on the northern focal hemisphere in Fig. 16c. Other than the E-W compression the reverse fault with the N-S compression is observed for some aftershocks of the 1964 Niigata Earthquake and in a mesh of the longitude from 142° to 143°E. The vertical extension and hrizontal E-W compressions are predominantly observed, although the N-S and E-W compressions are

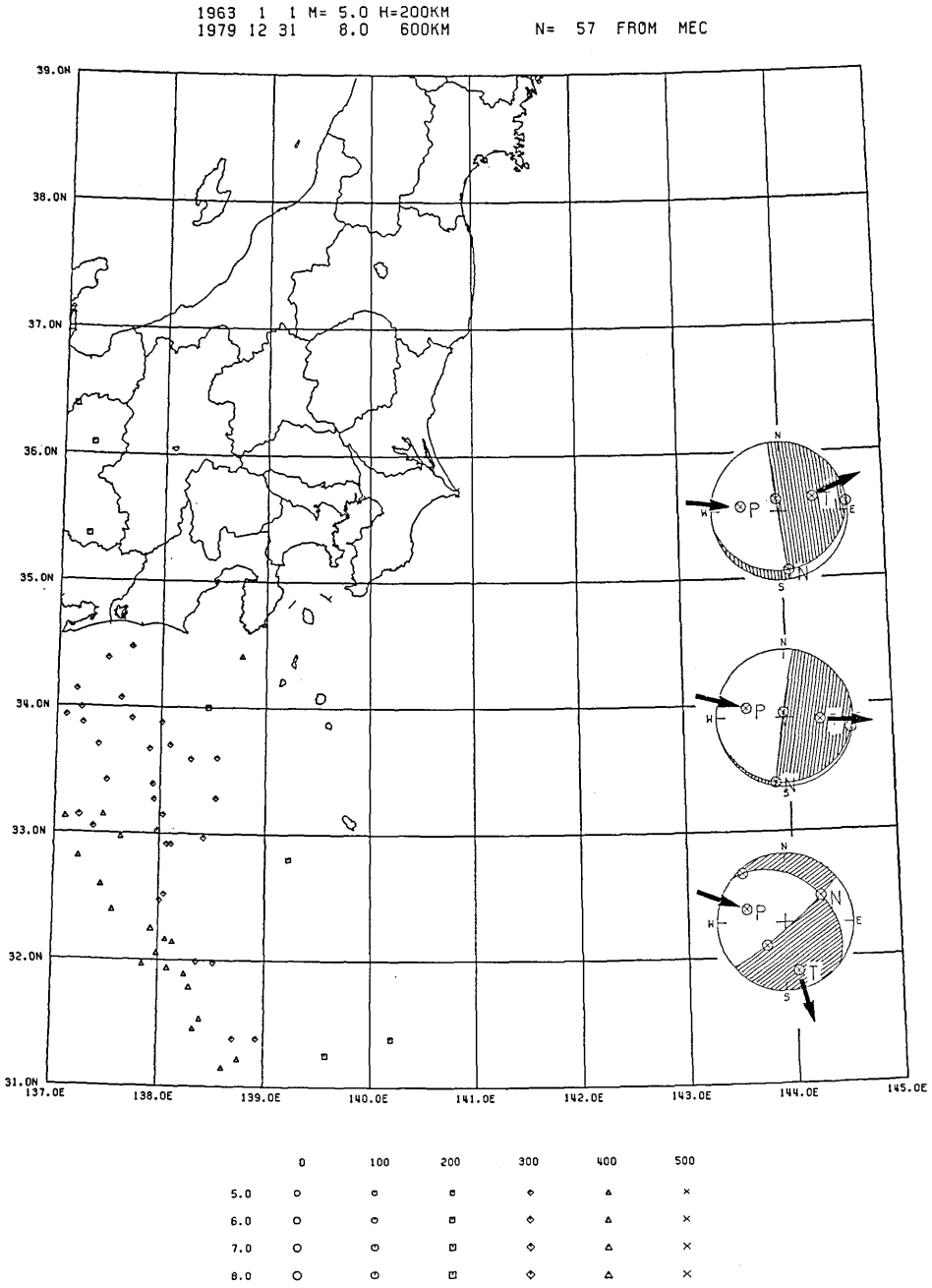

Fig. 15. Average fault-plane solutions of deeper mantle earthquakes (h=200–600 km) in and around the Kanto District. Focal depths are classified for every 100 km as shown in the legend.

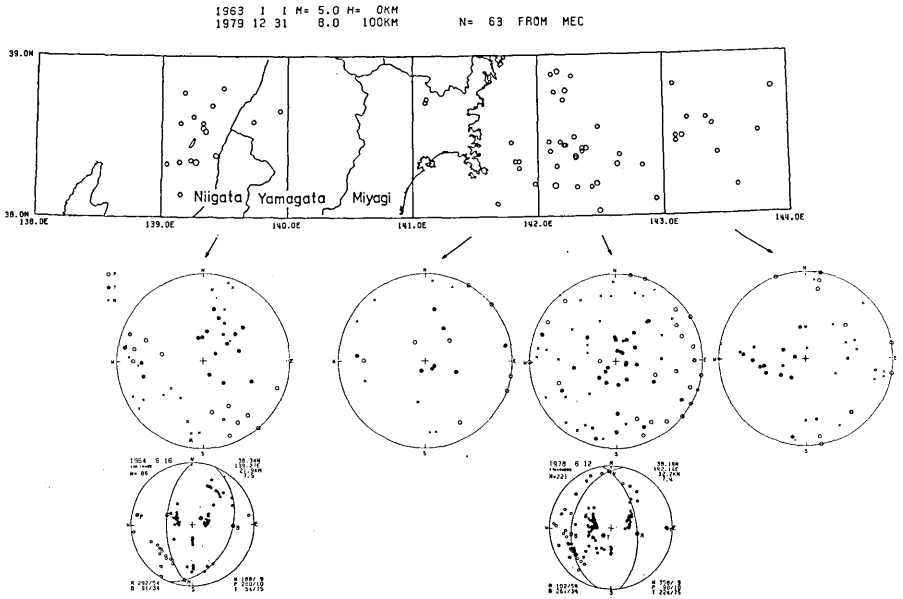

Fig. 16a. Summary of fault-plane solutions of crustal and subcrustal earthquakes (h= 0–100 km) along the E-W section from latitudes 38° to 39°N. The top denotes the epicenter distribution of earthquakes whose faultplane solutions are determined. The middle part shows summaries of fault-plane solutions for earthquakes within 1°-mesh of the longitude along the E-W section. The bottom shows the focal mechanisms and first-motion data of the 1964 Niigata and 1978 Off Miyagi Prefecture Earthquakes.

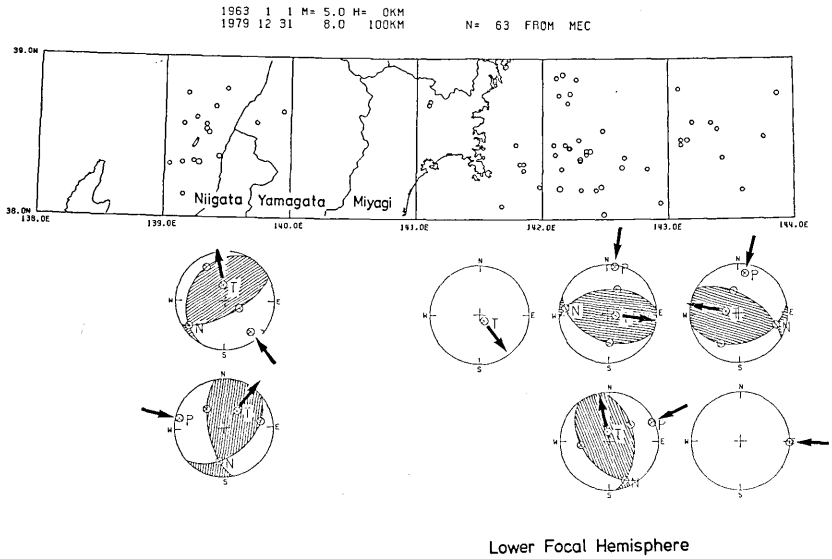

Fig. 16b. Equal-area projection of average fault-plane solutions on the lower focal hemisphere for earthquakes along the section between latitudes 38° and 39°.

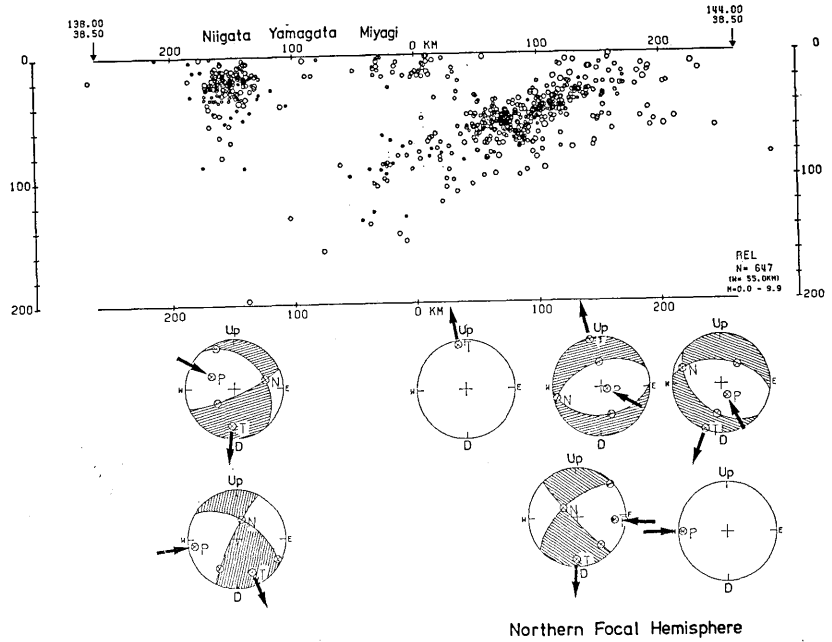

Fig. 16c. Equal-area projection of average fault-plane solutions on the northern focal hemisphere for earthquakes along the E-W section between latitudes 38° and 39°N. The top denotes the depth distribution along the E-W section of the relocated hypocenters by correcting the Pn station biases (MAKI, 1981a).

also observed.

In Fig. 17a the spatial variation of fault-plane solutions along a section of latitude 36° and 37°N are summarized. This section includes the Matsushiro Earthquake Swarm (1965 to 1968) from 138° to 139°E, the Kashimanada Earthquake on September 18, 1965 and earthquakes in the southwestern part of the Ibaraki Prefecture around 140°E. In the Kashimanada region from 141° to 142°E, a variety of azimuths of compression from NE to SE are observed. The horizontal E-W extension is observed for earthquakes located far east off the Ibaraki Prefecture from 141° to 143°E. Most of the earthquakes in the Matsushiro Swarm are interpreted by the strike-slip with the E-W compression. Fig. 17b shows schematic diagrams of average fault-plane solutions within each mesh along this section. Reverse faults with the horizontal compression of NW-SE, NE-SW and E-W directions are predominant. Fig. 17c compares schematically the northern focal hemisphere of average fault-plane solutions with the depth variation of the relocated hypocenters. Most of the earthquakes along this section have the reverse fault along the plane dipping to the west.

Along this section two intense clusters of subcrustal hypocenters are found beneath the southwestern part of the Ibaraki Prefecture

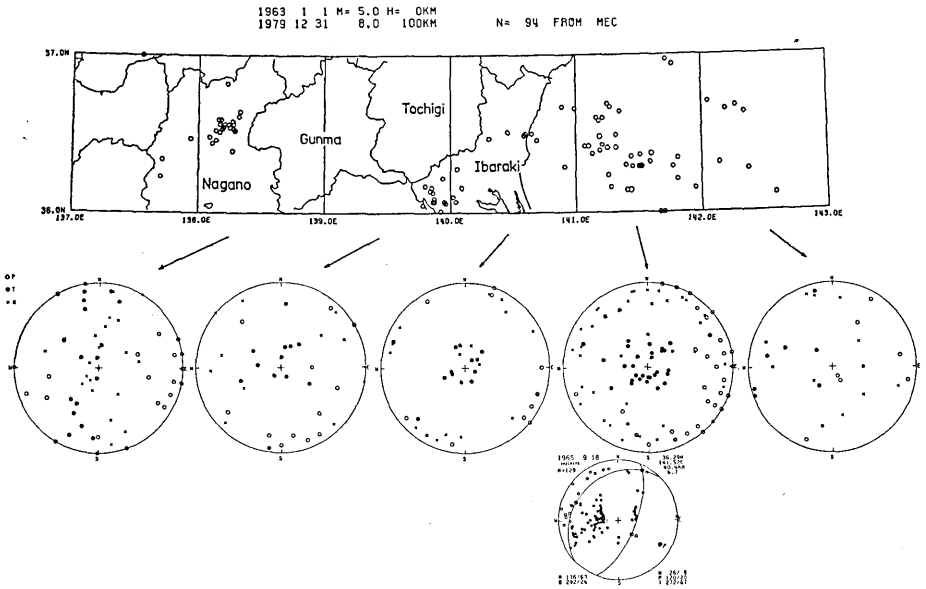

Fig. 17a. Summary of fault-plane solutions of crust and subcrustal earthquakes (h= 0–100 km) along the E-W section of latitudes 36° and 37°N. The bottom denotes the focal mechanisms and first-motion data for the 1965 Kashimanada (Off Ibaraki prefecture) Earthquake.

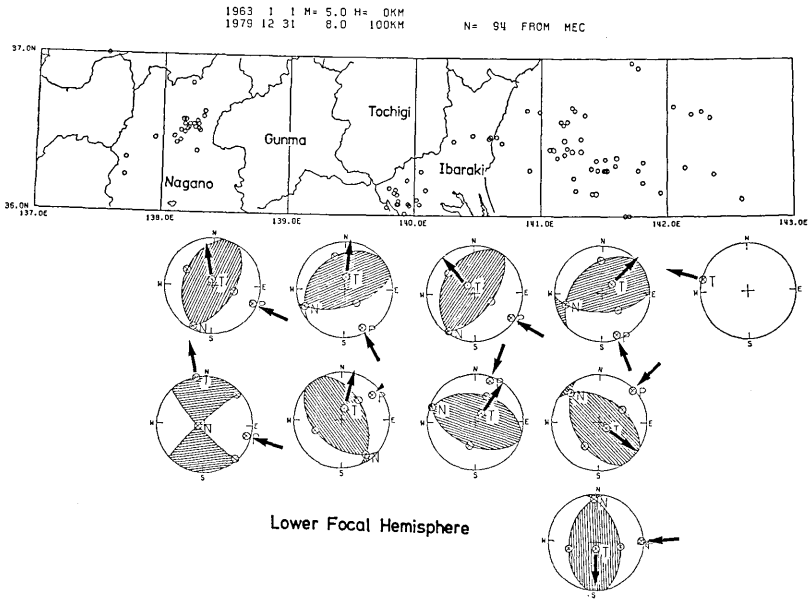

Fig. 17b. Equal-area projection of average fault-plane solutions on the lower focal hemisphere for earthquakes along the E-W section between latitudes of 36° and 37°N.

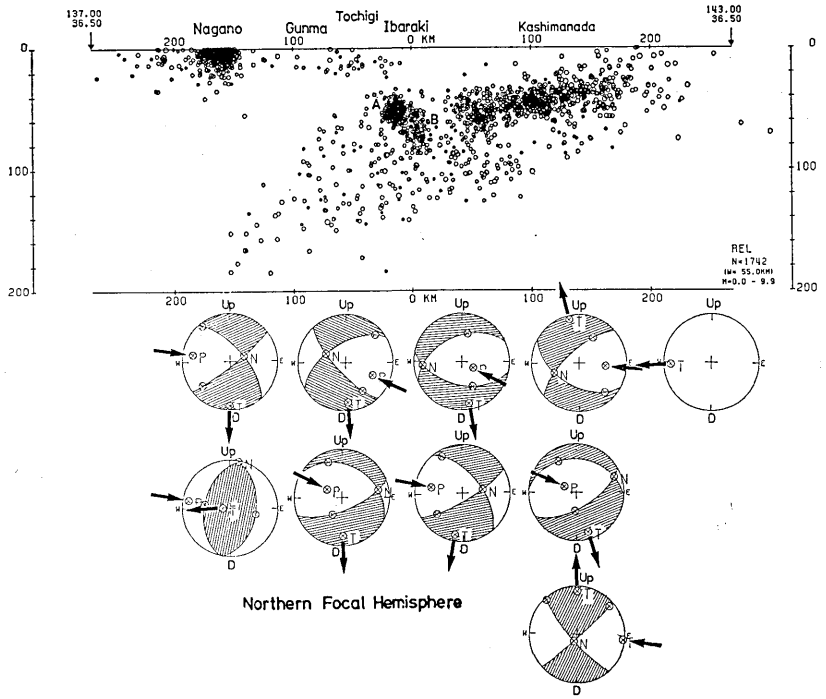

Fig. 17c. Equal-area projection of average fault-plane solutions on the northern focal hemisphere for earthquakes along the E-W section between latitudes 36° and 37°N. Two groups of earthquakes are distinguished, namely earthquakes of group "A" are located at the shallower depths on the western side of 140°E, and earthquakes of group "B" are located at deeper part on the eastern side of 140°E.

(MAKI *et al.*, 1980; MAKI and TSUMURA, 1980; MAKI, 1981b). One cluster is located at the shallower part on the western side of the longitude 140°E (A in Fig. 17c) and the other in the deeper part on the eastern side (B in Fig. 17c). Both groups commonly show the reverse fault with the NW-SE compression. MAKI *et al.*, (1980) preferred the vertical slip along the N-S striking plane for the deeper earthquakes on the eastern side of 140°E due to the vertical alignment of hypocenters within the seismic zone, and the low-angle thrust faulting for the shallower ones due to the agreement with the inclined seismic zone along the upper boundary of the Pacific plate.

5. Structure of earthquake-generating stress

Average fault-plane solutions of earthquakes within some extent have been used for studying regional variations of focal mechanisms in the previous chapters. The size and location of source regions with similar focal mechanisms may be discussed for the smaller extent. In this

chapter spatial variation of individual fault-plane solutions will be studied by classifying them into several types of faulting. Fault-plane solutions are here classified systematically on the basis of dip angles and azimuths of pressure and tension axes and null vector.

Fig. 18 shows seven types of fault-plane solutions of earthquakes with depths from 0 to 200 km. Open and solid circles denote axes of maximum compression and tension, and crosses denote null vector, respectively. The reverse faults with steeply dipping axes of maximum tension ($\delta_T \geqq 45°$) are divided into two groups with the NW-SE ($n=147$) and NE-SW ($n=113$) compression (top). The normal faults with steeply dipping axes of maximum pressure ($\delta_P \geqq 45°$) are also divided into two groups with the NW-SE ($n=33$) and NE-SW ($n=37$) extension (second). The third line shows two kinds of strike-slip with steeply dipping null vectors ($\delta_N \geqq 45°$) of NW-SE ($n=57$) and NE-SW ($n=50$) compression. Seventeen solutions are left in the final classification (bottom).

The epicenter distribution of crustal earthquakes ($h=0-40$ km) classified by fault types is shown in Fig. 19a. The reverse faults, whose epicenters are shown by solid symbols, are predominant in the northern region, and the strike-slip and normal fault, shown by open and cross symbols, are frequently observed in the southern region of the Kanto District and vicinity. Earthquakes located east off the Boso Peninsula and south off the Kanto District undergo the extensional stress. The geographical distribution of faulting types is shown in Fig. 19b for subcrustal earthquakes ($h=40-100$ km). Earthquakes in the coastal region on the Pacific side show the reverse fault as same as the crustal earthquakes. The reverse faults are also seen for earthquakes located east off the Hachijojima Island. Earthquakes with the horizontal extension are observed near the trench and south off the Kanto district.

The normal faults with the E-W extension were seen for earthquakes located beyond the Japan Trench on Aug. 25, 1974 (M 5.8) and and June 15, 1975 (M 5.9), and on the western side of the Japan Trench on Sep. 10, 1971 (M 5.2), Mar. 27, 1973 (M 5.0) and Aug. 12, 1979 (M 5.7). Earthquakes located directly beneath the Japan Trench showed the normal fault with the N-S extension on Oct. 29, 1968 (M 5.4) and Mar. 19, 1972 (M 5.7), and the vertical slip with the western side downgoing on Apr. 22, 1966 (M 5.8) and June 18, 1968 (M 6.0). The strike-slip is seen for earthquakes located around the Boso triple junction on Mar. 1, 1964 (M 5.5) and Aug. 10, 1973 (M 5.4). A few different focal mechanisms other than the reverse fault are observed, such as the normal fault of an earthquake on Jan. 27, 1965 (M 5.6)

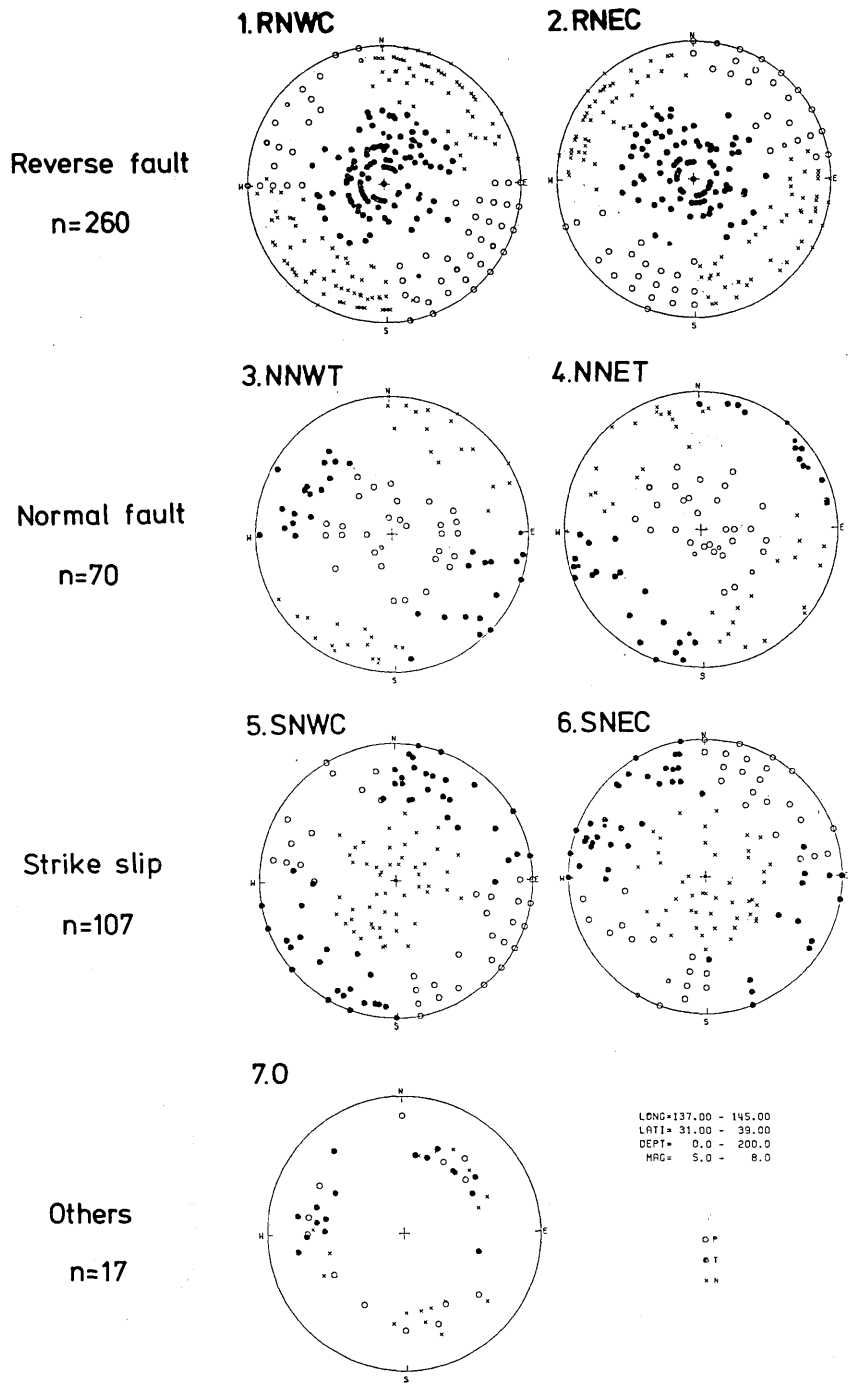

Fig. 18. Seven types of fault-plane solutions for crust and mantle earthquakes with depths of 0 to 200km. Axes of maximum pressure and tension are denoted by open and solid circles, and null vectors by crosses. (1) RNWC: reverse fault with NW-SE compression, (2) RNEC: reverse fault with NE-SW compression, (3) NNWT: normal fault with NW-SE extension, (4) NNET: normal fault with NE-SW extension, (5) SNWC: strike-slip with NW-SE compression, (6) SNEC: strike-slip with NE-SW compression, (7) O: others.

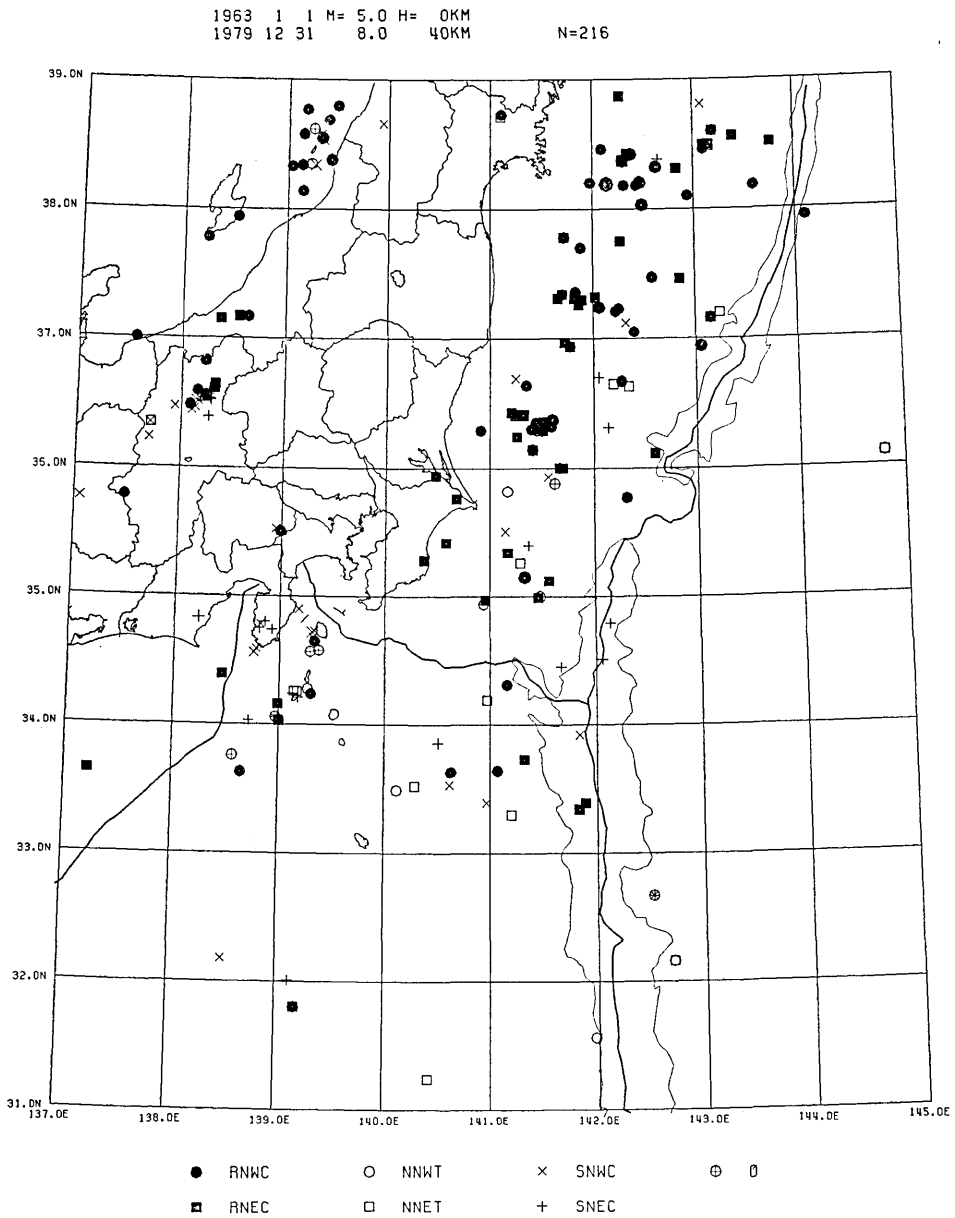

Fig. 19. Geographical distribution of fault types of crustal earthquakes (n=216 solutions), classified into seven types as seen in Fig. 18. Solid and open symbols denote reverse and normal faults, and strike-slips are shown by crosses. Each type of faulting is divided into two ones based on azimuths of P and T axes, and shown by circles and squares as in Fig. 18. Epicenters with multiple solutions are shown by duplicated symbols.

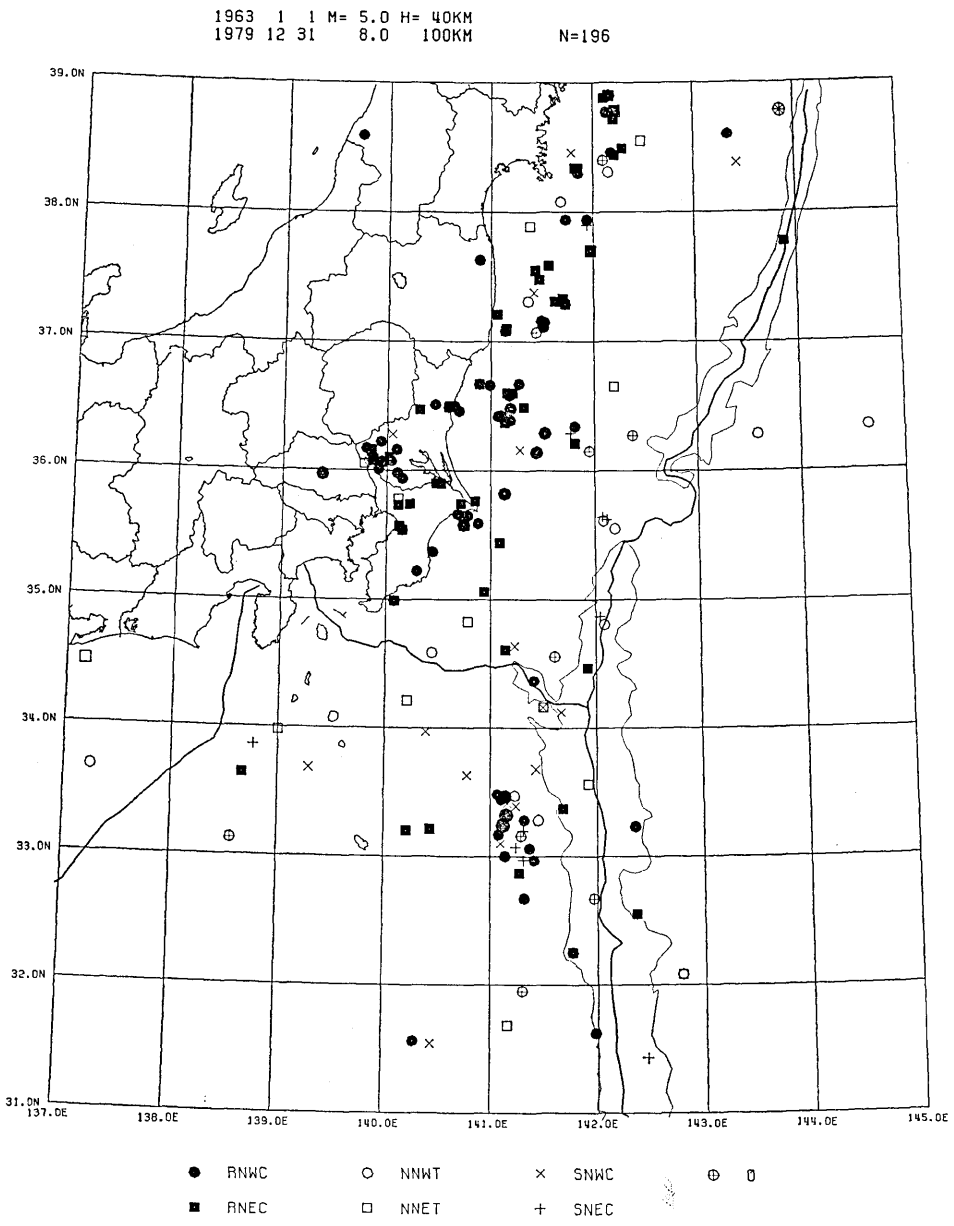

Fig. 19. Geographical distribution of fault types of subcrustal earthquakes (n=196 solutions), classified into seven types as seen in Fig. 18.

and the strike-slip on Mar. 19, 1967 (M 5.5).

Depth variations of fault types along the E-W section of the 60 km width on both sides are shown in Fig. 20 (a to f). Locations of the trench axis are shown by thick arrowheads. In general earthquakes along the lower plane of the double seismic zone tend to show

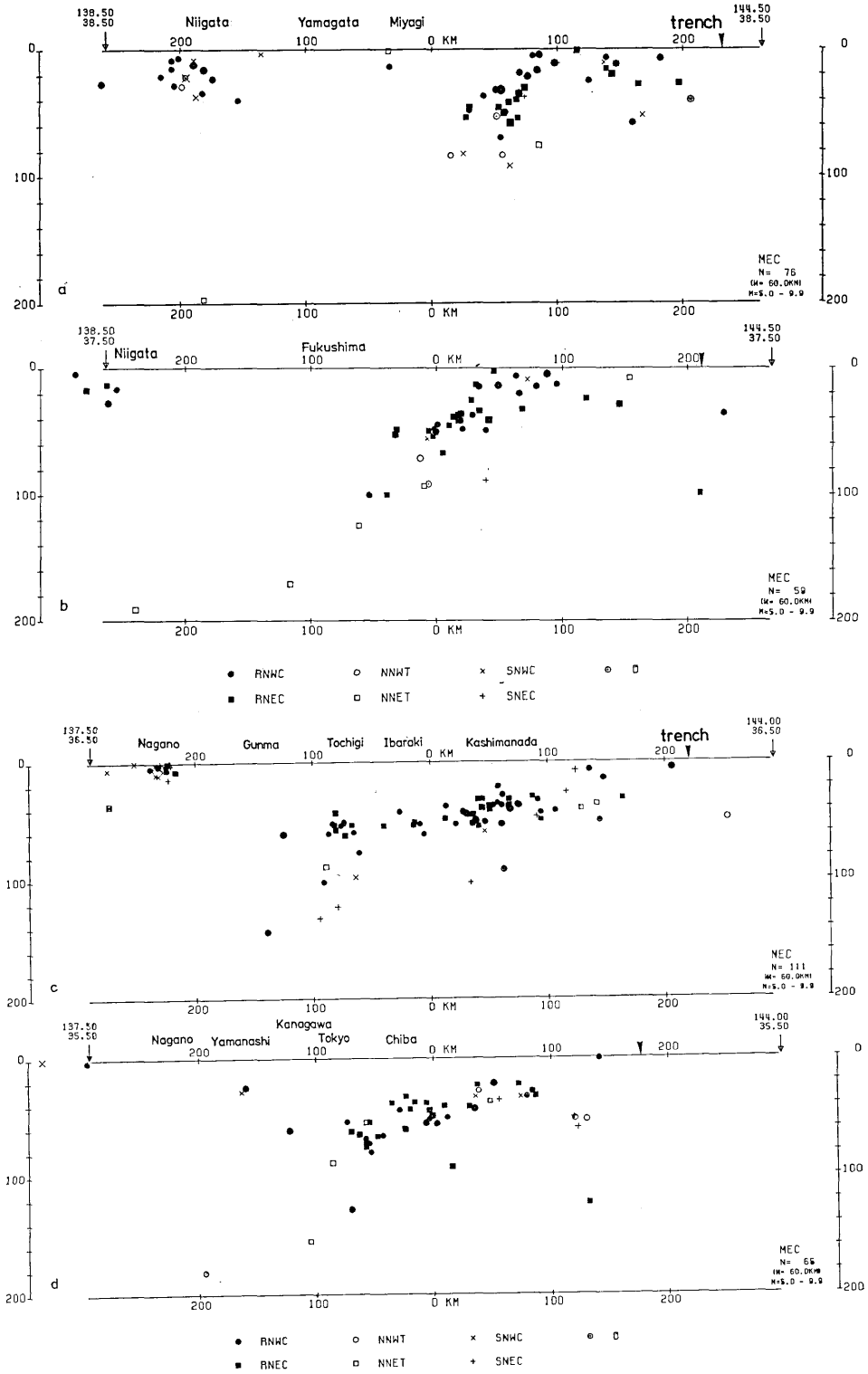
138.50
38.50
Niigata
Yamagata
Miyagi
trench
144.50
38.50
0 KM
MEC
N= 76
M=5.0 - 9.9
a
138.50
37.50
Niigata
Fukushima
144.50
37.50
MEC
N= 59
M=5.0 - 9.9
b
RNWC
RNEC
NNWT
NNET
SNWC
SNEC
137.50
36.50
Nagano
Gunma
Tochigi
Ibaraki
Kashimanada
trench
144.00
36.50
MEC
N= 111
M=5.0 - 9.9
c
137.50
35.50
Nagano
Yamanashi
Kanagawa
Tokyo
Chiba
144.00
35.50
MEC
N= 65
M=5.0 - 9.9
d

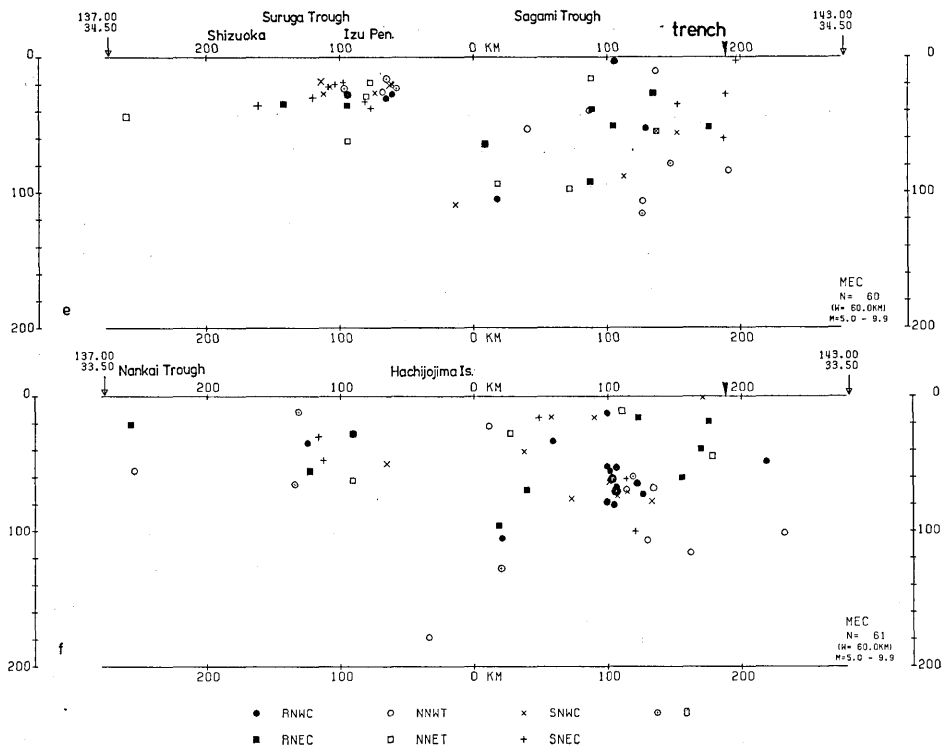

Fig. 20. Depth distribution of fault types of earthquakes along the E–W sections of the 60 km width on both sides between the following two points (thin arrows), (a) (138.5°E, 38.5°N) and (144.5°E, 38.5°N), (b) (138.5°E, 37.5°N) and (144.5°E, 37.5°N), (c) (137.5°E, 36.5°N) and (144.0°E, 36.5°N), (d) (137.5°E, 35.5°N) and (144.0°E, 35.5°N), (e) (137.0°E, 34.5°N) and (143.0°E, 34.5°N), and (f) (137.0°E, 33.5°N) and (143.0°E, 33.5°N). Locations of the trench and trough axes are shown by thick arrowheads.

the normal fault or strike-slip. Earthquakes located south off the Kanto District have a variety of focal mechanisms. Shallow earthquakes in this region show the normal fault and strike-slip.

A significant contrast in the seismicity and focal mechanisms along the plate boundary is recognized between the northern and southern regions along the Japan Trench as indicated by KANAMORI (1977) and UYEDA and KANAMORI (1979). In the coastal region on the Pacific side from Northeast Japan to the Boso Peninsula, earthquakes with the reverse fault are distinctively observed along the boundary of the Pacific and Eurasian Plates. Such a zone of reverse faults indicates the strong coupling of the descending and overriding plates. On the other hand the scattered hypocenters in the depth distribution and infrequent reverse faults along the upper boundary of the inclined seismic zone in the Izu-Bonin region suggest the decoupling of the Pacific and Philippine Sea Plates.

6. Discussion and conclusion

Fault-plane solutions and their confidence regions were obtained by the new numerical method for 454 earthquakes ($M \geqq 5.0$), which occurred in and around the Kanto District during 17 years from 1963 to 1979. For five earthquakes useful solutions with scores of 95% or more cannot be obtained. The fault-plane solutions in the present study are considered to be determined by a completely objective method. Unique solutions are obtained for many earthquakes, but for some earthquakes multiple solutions are possible. These fault-plane solutions suggest spatial variations of earthquake-generating stress or complicated patterns of the tectonic process in and around the Kanto District. Earthquakes in the Kanto District are located at a variety of relative locations, as along the plate boundaries and within the descending and overriding plates.

According to individual fault-plane solutions of 38 larger earthquakes with magnitudes of 6.0 or more, average fault-plane solutions and faulting types, focal mechanisms of earthquakes in and around the Kanto Districh are summarized into three types, namely (1) reverse faulting with the vertical extension and horizontal compression, (2) strike-slip with the N-S and E-W compression, and (3) normal faulting with the horizontal E-W extension. The first type is predominant for earthquakes in the entire region, especially on the Pacific side. The second type is observed for shallow earthquakes near the Izu Peninsula and Izu Oshima Island and in the inland region. The third type is observed for earthquakes located south and southeast off the Kanto District.

Regional variations are derived by summarizing and averaging fault-plane solutions of earthquakes within specific regions. Average fault-plane solutions were obtained by the arithmetic means of direction cosines of axes of maximum pressure and tension and by computational location of other axes. By preliminary restraining of solutions several representative focal mechanisms could be obtained.

For earthquakes with focal depths down to 100 km, the reverse fault of the vertical extension with the horizontal E-W compression are predominant for all the regions, although the axes of maximum compression are variable. The horizontal E-W extension is observed for shallow earthquakes in the southwestern quarter, where a strike-slip with the N-S compression or a normal fault. Earthquakes in the inland region show the strike-slip with the E-W compression. A systematic variation of tension axes is observed for the reverse faults along the E-W section of latitude from 38° and 39°N. Sizes of the source region with regular focal mechanisms are variable from the

northern and southern Kanto District. The horizontal E-W extension is also observed for some subcrustal earthquakes on the Pacific side. This type of focal mechanism means the "down-dip extension" along the lower plane of the double seismic zone. The mantle earthquakes with focal depths from 400 to 600 km show the down-dip compression along the inclined seismic zone.

Source regions with regular focal mechanisms were derived from the geographical distribution of faulting types which are classified systematically by dip angles and azimuths of P, T and N axes. Thrust faults are predominant along the plate boundary between the Pacific and Eurasian Plates below the Pacific coast of Miyagi, Fukushima, Ibaraki and Chiba Prefectures. Thrust faults are also found for crustal earthquakes on the Japan Sea side in Niigata Prefecture, and for deeper earthquakes in the 1972 Hachijojima Earthquake region.

The inclined seismic zone observed in Northeast Japan is not seen for earthquakes occurred in the Izu-Bonin Islands. Strike-slip and normal fault are seen for crustal and subcrustal earthquakes in this region. Most of the deep-focus earthquakes below the Kanto District and Izu-Bonin Islands show the down-dip compression along the inclined seismic zone (ISACKS and MOLNAR, 1971). The down-dip extension along the inclined seismic zone is also observed for earthquakes located on the lower side of the seismic zone.

The Kanto District is also located at the transition zone of different types of the trench-arc systems. Different processes of the tectonics between Northeast Japan and the Izu Bonin Island arc systems have heen pointed out by KANAMORI (1971b, 1977) and interpreted by the existence of bathymetric rises or seamounts (KELLEHER and MCCANN, 1976). For regions accompanied by the bathymetric rises, the absence of large low-angle thrust earthquakes, infrequent large earthquakes and hypocenter gaps in the intermediate-depth are commonly observed in a global survey (KELLEHER and MCCANN, 1976). UYEDA and KANAMORI (1979) showed the existence of two types of trench-arc system classified according to the difference in coupling between descending and overriding plates, namely (1) the Chilean type with the strong coupling, and (2) the Mariana type with the decoupling boundary. They also mentioned the tensional stress in the back-arc region for the Mariana type. Mechanisms of these types are interpreted by the differences in the evolutional stage (KANAMORI, 1971b, 1977), the anchored slab (UYEDA and KANAMORI, 1979), or the intercept of subduction due to the bathymetric rises (KELLEHER and MCCANN, 1976). Earthquake mechanisms of the thrust faulting in the Kanto District and Northeast Japan are produced by the descent of

the Pacific Plate underneath the Eurasian Plate. On the other hand earthquakes in the Izu-Bonin region are produced by the stress-free state or extensional stress due to the decoupling of the Philippine Sea Plate with the Pacific Plate.

Great normal faults have been observed for the 1933 Sanriku Earthquake (KANAMORI, 1971a), the 1965 Rat Island Earthquakes (STAUDER, 1968; ABE, 1972) and the 1969 Christmas Day Earthquakes (STEIN *et al.*, 1982). The normal faults occurring near the trench were interpreted by the failure (detachment) due to the weight of the descending slab (KANAMORI, 1971a, b, 1977) and bending (flexture) of the downgoing slabs (CHEN and FORSYTH, 1978; CHAPPLE and FORSYTH, 1979). Earthquakes in the upper part of the downgoing slabs are commonly expected as the tensional faulting in both models, but those in the deeper part might be helpful to discriminate the two models (STEIN *et al.*, 1982). Earthquakes with tensional stresses below the Japan Trench off the Kanto District and Northeast Japan are located not only near the surface but also near the bottom of the descending slab. Then these tensional events cannot be interpreted only by the near-surface bending.

Intermediate-depth earthquakes along the double-planed seismic zone show two types of focal mechanisms, namely the down-dip compression along the upper plane and the down-dip extension along the lower plane (UMINO and HASEGAWA, 1975, 1982; ISACKS and BARAZANGI, 1977; HASEGAWA *et al.*, 1978a, b). In the Kanto District such a double seismic zone was first found by TSUMURA (1973). The double seismic zone with such opposite stresses has been interpreted by the unbending of the downgoing slab (ENGDAHL and SCHOLZ, 1977) and the sagging of the slab (SLEEP, 1977). Focal mechanisms of intermediate-depth earthquakes, along the lower plane of the double seismic zone below the Kanto District, show not only the "down-dip extension" but also the strike-slip or lower-angle extension. More complicated patterns of earthquake-generating stress should be taken into consideration for the unbending or sagging model. Some intermediate-depth earthquakes show some different types of focal mechanisms. ISACKS and BARAZANGI (1977) showed a possible segmentation of descending slab in the intermediate-depths, or a contortion, off-set and tear of the slabs. STEIN *et al.*, (1982) showed the reactivation of the fossil faulting in the deeper part in the Lesser Antilles Arc. The regional variations of focal mechanisms with relation to the slab configuration were presented by STAUDER (1973, 1975), FORSYTH (1975), CARDWELL and ISACKS (1978) and PASCAL *et al.*, (1978). Difficulties in interpreting some focal mechanisms in Chile and Peru were mentioned by

STAUDER (1973, 1975).

A variety of focal mechanisms are observed in the Kanto District and vicinity. Here earthquakes are located at various relative locations as along the plate boundaries of the Pacific Plate with the Eurasian and Philippine Sea Plates, along the lower plane of the double seismic zone of the Pacific Plate and near the trench. Smaller earthquakes may be produced by the local stress rather than the tectonic stress for large earthquakes. Analyses of focal mechanisms for more earthquakes by a unified and objective method are required for detailed studies of earthquake-generating stress, together with the precise locations of hypocenters.

Acknowledgments

The author would like to acknowledg Prof. Tokuji Utsu and Kazuaki Nakamura for reviewing the manuscript. Dr. Ichiro Kawasaki of theToyama University made helpful comments. Several comments and suggestive discussions at the Utsu Seminar are also acknowledged. Computation and drafting were done by using the IBM 370-3130 of the Earthquake Prediction Data Center, Earthquake Research Institute, the University of Tokyo.

References

ABE, K., 1972, Lithospheric normal faulting beneath the Aleutian trench, *Phys. Earth Planet. Inter.*, **5**, 190-198.

ABE, K., 1975a, Re-examination of the fault model for the Niigata Earthquake of 1964, *Journ. Phys. Earth*, **23**, 349-366.

ABE, K., 1975b, Static and dynamic fault parameters of the Saitama Earthquake of July 1, 1968, *Tectonophysics*, **27**, 223-238.

ABE, K., 1978, Dislocations, source dimensions and stresses associated with earthquakes in the Izu Peninsula, Japan, *Journ. Phys. Earth*, **26**, 253-274.

ANDO, M. and T. MIKUMO, 1974, Read on Oct. 11, 1974, at the semiannual meeting of the Seismological Society of Japan.

AOKI, H., 1974, Plate tectonics of arc-junction at Central Japan, *Journ. Phys. Earth*, **22**, 141-161.

CARDWELL, R.K. and B.L. ISACKS, 1978, Geometry of the subducted lithosphere beneath the Banda Sea in Eastern Indonesia from seismicity and fault plane solutions, *Journ. Geophys. Res.*, **83**, 2825-2838.

CHAPPLE, W. M. and D. W. FORSYTH, 1979, Earthquakes and bending of plates at trenches, *Journ. Geophys. Res.*, **84**, 6729-6749.

CHEN, T. and D. W. FORSYTH, 1978, A detailed study of two earthquakes seaward of the Tonga Trench: Implications for mechanical behavior of the oceanic lithosphere, *Journ. Geophys. Res.*, **83**, 4995-5003.

ENGDAHL, E.R. and C.H. SCHOLZ, 1977, A double Benioff zone beneath the central Aleutians: An unbending of the lithosphere, *Geophys. Res. Lett.*, **4**, 473-476.

FARA, H. D., 1964, A new catalogue of earthquake fault plane solutions, *Bull. Seism. Soc. Amer.*, **54**, 1491-1517.

FARA, H.D. and A.E. SHEIDEGGER, 1963, An eigenvalue method for the statistical evaluation of fault plane solutions of earthquakes, *Bull. Seism. Soc. Amer.*, **53**, 811–816.

FORSYTH, D. W., 1975, Fault plane solutions and tectonics of the South Atlantic and Scotia Sea, *Journ. Geophys. Res.*, **80**, 1429–1443.

FUJITA, K. and H. KANAMORI, 1981, Double seismic zones and stresses of intermediate depth earthquake, *Geophys. Journ. Roy. astr. Soc.*, **66**, 131–156.

HASEGAWA, A., N. UMINO and A. TAKAGI, 1978a, Double-planed structure of the deep seismic zone in the northeastern Japan arc, *Tectonophysics*, **47**, 43–58.

HASEGAWA, A., N. UMINO and A. TAKAGI, 1978b, Double-planed deep seismic zone and upper-mantle structure in the Northeastern Japan Arc, *Geophys. Journ. Roy. astr. Soc.*, **54**, 281–296.

HIRASAWA, T., 1965, Source mechanism of the Niigata earthquake of June 16, 1964, as derived from body waves, *Journ. Phys. Earth*, **13**, 35–66.

ICHIKAWA, M., 1962, Statistical investigation of earthquake mechansism in Kwanto District, *Geophys. Mag.*, **31**, 243–256.

ICHIKAWA, M., 1970a, Seismic activities at the junction of Izu-Mariana and Southwestern Honshu Arcs. *Geophys. Mag.*, **35**, 55–69.

ICHIKAWA, M., 1970b, Earthquakes in the southern part of Kwanto, Central Japan, *Journ. Geol.* (*Chigaku Zasshi*), **79**, 151–166 (in Japanese).

ICHIKAWA, M., 1971, Reanalyses of mechanisms of earthquakes which occurred in and near Japan, and statistical studies on the nodal plane solutions obtained, 1926–1968, *Geophys. Mag.*, **35**, 207–274.

ICHIKAWA, M., 1979, Some problems in the focal mechanism in and near Japan, *Geophys. Mag.*, **39**, 1–22.

ISACKS, B.L. and M. BARAZANGI, 1977, Geometry of Benioff zone: Lateral segmentation and downwards bending of the subducted lithosphere, in "*Island Arcs, Deep Sea Trenches and Back-Arc Basins*", Maurice Ewing Ser., vol. 1, edited by M. Talwani and W.C. Pitman III, AGU, Washington, D.C., pp. 99–114.

ISACKS, B. and P. MOLNAR, 1971, Distribution of stresses in the descending lithosphere from a global survey of focal mechanism solution of mantle earthquakes, *Rev. Geophys. Space Phys.*, **9**, 103–174.

JMA (THE JAPAN METEOROLOGICAL AGENCY), 1976, 1977, 1978, 1979, 1980, 1982, List of nodal plane solutions for earthquakes occurring in 1973, 1974, 1975, 1976, 1977 and 1978, Monthly seismological bulletins of the JMA.

KANAMORI, H., 1971a, Seismological evidence for a lithospheric normal faulting—The Sanriku earthquake of 1933, *Phys. Earth Planet. Inter.*, **4**, 289–300.

KANAMORI, H., 1971b, Great earthquakes at island arcs and the lithosphere, *Tectonophysics*, **12**, 187–198.

KANAMORI, H., 1977, Seismic and aseismic slip along subduction zones and their tectonic implications, in "*Island Arcs, Deep Sea Trenches and Back-Arc Basins*", Maurice Ewing Ser., vol. 1, edited by M. Talwani and W.C. Pitman III, AGU, Washington, D.C., pp. 162–174.

KELLEHER, J. and W. MCCANN, 1976, Buoyant zones, great earthquakes, and unstable boundaries of subduction, *Journ. Geophys. Res.*, **81**, 4885–4896.

MAKI, T., 1974, On the earthquake mechanism of the Izu-Hanto-Oki Earthquake of 1974, *Prelim. Rep. Earthq. Res. Inst.*, **14**, 23–36 (in Japanese).

MAKI, T., 1975a, Read on May 15, 1975, at the semi-annual meeting of the Seismological Society of Japan.

MAKI, T., 1975b, Read on Oct. 7, 1975, at the semi-annual meeting of the Seismological Society of Japan.

MAKI, T., 1981a, Regional variation of Pn residuals and its application to relocation of earthquakes in and around the Kanto District, *Bull. Earthq. Res.* Inst., **56**, 309–346.

MAKI, T., 1981b, Earthquake mechanisms of subcrustal earthquakes beneath the Kanto

District, *Memoirs Geol. Soc. Japan*, **20**, 259-266 (in Japanese).

MAKI, T., 1982, Numerical estimation of confidence region of fault-plane solutions, *Bull. Earthq. Res. Inst.*, **57**, 193-220.

MAKI, T., I. KAWASAKI and A. HORIE, 1980, Earthquake mechanisms associated with the conjunction of the sinking plates beneath the Kanto District, Central Japan, *Bull. Earthq. Res. Inst.*, **55**, 577-600.

MAKI, T. and K. TSUMURA, 1980, On seismic fault-systems derived from the spatial distribution and mechanisms of the earthquakes in the Kanto District, *Journ. Anal. Res. Data Natur. Disast.*, **7**, 47-60 (in Japanese).

MATSUZAKI, T. and I. KAWASAKI, Read on Oct. 11, 1974, at the semi-annual meeting of the Seismological Society of Japan.

MIKUMO, T., T., 1973, Faulting mechanism of the Gifu Earthquake of September 9, 1969, and some related problems, *Journ. Phys. Earth*, **21**, 191-212.

NAKAMURA, K., 1979, σH_{max} Trajectories east of Suruga Trough, Japan—as effect of flexure of lithospheric plate, *Zishin* II, **32**, 370-372 (in Japanese).

PASCAL, G., B.L. ISACKS, M. BARAZANGI and J. DUBOIS, 1978, Precise relocations of earthquakes and seismotectonics of the New Hebrides Island Arc, *Journ. Geophys. Res.*, **83**, 4957-4973.

RITSEMA, A.R. and J.G.J. SCHOLTE, 1961, Note on the determination of the best-fitting plane for a given set of directions, *Geofis. Pura et Appl.*, **49**, 13-14.

SASATANI, T., 1971, Source mechanism of two shallow earthquakes as derived from body waves, *Geophys. Bull. Hokkaido Univ.*, **26**, 109-132 (in Japanese).

SASATANI, T., 1976, Mechanism of mantle earthquakes near the junction of the Kurile and the Northern Honshu Arcs, *Journ. Phys. Earth*, **22**, 141-161.

SCHEIDEGGER, A.E., 1958, Tectonophysical significance of fault plane solutions of earthquakes, *Geofis. Pura et Appl.*, **39**, 19-25.

SENO, T., K. SHIMAZAKI, P. SOMERVILLE, K. SUDO and T. EGUCHI, 1980, Rupture process of the Miyagi-Oki, Japan, Earthquake of June 12, 1978, *Phys. Earth Planet. Int.*, **23**, 39-61.

SHIMAZAKI, K. and P. SOMERVILLE, 1978, Summary of the static and dynamic parameters of the Izu-Oshima-Kinkai Earthquake of January 14, 1978, *Bull. Earthq. Res. Inst.*, **53**, 613-628.

SHIMAZAKI, K. and P. SOMERVILLE, 1979, Static and dynamic parameters of the Izu-Oshima, Japan Earthquake of January 14, 1978, *Bull. Seism. Soc. Amer.*, **69**, 1343-1378.

SHIONO, K., 1977, Focal mechanism of major earthquakes in southwest Japan and their tectonic significance, *Journ. Phys. Earth*, **25**, 1-26.

SHIONO, K. and T. MIKUMO, 1975, Tectonic implications of subcrustal normal faulting earthquakes in the western Shikoku region, *Journ. Phys. Earth*, **23**, 257-278.

SHIONO, K., T. MIKUMO and Y. ISHIKAWA, 1979, Earthquake mechanisms in Hyuganada and the Ryukyu arc and their geologic significance, *Journ. Phys. Earth*, **28**, 17-43.

SLEEP, N.H., 1979, The double seismic zone in downgoing slabs and the viscosity of the mesosphere, *Journ. Geophys. Res.*, **84**, 4565-4571.

SOMERVILLE, P., 1978, The accomodation of plate collision by deformation in the Izu block, Japan, *Bull. Earthq. Res. Inst.*, **53**, 629-648.

SOMERVILLE, P., 1980, Earthquake mechanisms at the head of the Philippine Sea Plate beneath the southern Kanto District, Japan, *Journ. Phys. Earth*, **28**, 293-308.

STAUDER, W., 1968, Tensional character of earthquake foci beneath the Aleutian trench with relation to sea-floor spreading, *Journ. Geophys. Res.*, **73**, 7693-7701.

STAUDER, W., 1973, Mechanism and spatial distribution of Chilean earthquakes with relation to subduction of the oceanic plate, *Journ. Geophys. Res.*, **78**, 5033-5061.

STAUDER, W., 1975, Subduction of the Nazca Plate under Peru as evidenced by focal mechanisms and by seismicity, *Journ. Geophys. Res.*, **80**, 1053-1064.

STAUDER, W. and L. MUALCHIN, 1976, Fault motion in the large earthquakes of the Kurile-

Kamchatka Arc and of the Kurile-Hokkaido Corner, *Journ. Geophys. Res.*, **81**, 297-308.

STEIN, S., J.F. ENGELN, D.A. WIENS, K. FUJITA and R.C. SPEED, 1982, Subduction seismicity and tectonics in the Lesser Antilles Arc, *Journ. Geophys. Res.*, **87**, 8642-8664.

TSUMURA, K., 1973, Microearthquake activity in the Kanto District, Publications for the 50th anniversary of the Great Kanto Earthquake, 1923, Earthq. Res. Inst., 67-87 (in Japanese).

UKAWA, M., 1982, Lateral stretching of the Philippine Sea Plate subduction along the Nankai-Suruga Trough, *Tectonics*, **1**, 543-571.

UMINO, N. and A. HASEGAWA, 1975, On the two-layered structure of deep seismic plane in Northeastern Japan Arc, *Zishin* II, **28**, 125-139 (in Japanese).

UMINO, N. and A. HASEGAWA, 1982, A detailed structure of the deep seismic zone and earthquake mechanism in the Northeast Japan Arc, *Zishin* II, **35**, 237-257 (in Japanese).

USAMI, T. and T. WATANABE, 1975, Definition and characteristics features of a seismically active region (earthquake nest) in the Kanto District, *Bull. Earthq. Res. Inst.*, **52**, 379-406 (in Japanese).

UYEDA, S. and H. KANAMORI, 1979, Back-arc opening and the mode of subduction, *Journ. Geophys. Res.*, **84**, 1049-1061.

VEITH, K.F., 1974, The relationship of island arc seismicity to plate tectonics, Ph. D. Thesis of Southern Methodist University.

VEITH, K.F., 1977, The nature of the dual zone of seismicity in the Kuriles Arc, *Trans. Amer. Geophys. Un.*, **58**, 1232.

WICKENS, A.J. and J.H. HODGSON, 1967, Computer reevaluation of earthquake mechanism solutions, 1922-1962, *Publ. Dom. Obs., Ottawa*, **33**, 1-560.

YOSHII, T., 1979a, Compilation of geophysical data around the Japanese Islands (I), *Bull. Earthq. Res. Inst.*, **54**, 75-117 (in Japanese).

YOSHII, T., 1979b, A detailed cross-section of the deep seismic zone beneath Northeastern Honshu, Japan, *Tectonophysics*, **55**, 349-360.

24. 関東地方における起震歪力の分布

地震研究所　牧　　正

数値解法によって関東地方と周辺に起った 454 個の地震 (1963～1979 年, $M \geqq 5.0$) の地震メカニズムを解析し起震歪力の分布を調べた．個々のメカニズム解・平均メカニズム・メカニズムタイプの分布が，Pn 観測点補正を行なって求められた高精度震源の分布と比較された．関東地方・東北日本の太平洋側と伊豆・小笠原諸島の間には起震歪力の分布に著しいコントラストがみられる．関東・東北日本の太平洋側では太平洋プレートの上面境界に沿った逆断層が卓越しているが，伊豆・小笠原諸島では西に傾き下がる地震帯も明瞭でなく種々のタイプのメカニズムがあらわれている．こうした相違は両地域における太平洋プレートの，ユーラシア・フィリピン海プレートとの結合の違いによると考えられる．関東・東北日本の地殻内・地殻直下の地震では水平東西の主圧力による逆断層が卓越しているが，個々の地震や地域によって主圧力軸の方位に変化がみられる．又主張力軸の傾きが東側で大きくなる地域変化もみられる．東西水平の主圧力は内陸部にもみられ，新潟地震では縦ずれ，松代地震では横ずれのメカニズムであらわれている．関東地方の南西部ではいくつかのタイプのメカニズムがみられる．伊豆半島・伊豆大島附近の極浅発地震では南北あるいは北西－南東主圧力の横ずれ断層が卓越し，関東南方沖では正断層があらわれる．これらのメカニズムでは水平東西の張力が共通している．マントル地震では主圧力軸が深発地震帯に沿って傾き下がるメカニズムの他，特に稍深発地震では地震帯に沿って傾き下がる主張力がみられる．これら 2 種類のメカニズムは二重深発地震面の上・下面にあたるが，特に下面に沿った主張力軸の方位や傾きは必ずしも地震帯に沿うものばかりではない．

Appendix

Equal-area projection of probable fault-plane solutions on the lower focal hemisphere (on the left-hand side) and first-motion data, and the most probable fault-plane solution (on the right-hand side). When useful scores of 95% or greater are not obtained in the first run, fault-plane solutions are determined after discarding apparently inconsistent first-motion data. Axes of maximum pressure and tension and null vector are denoted by "P", "T" ard "N". Solutions with scores of 99% or greater are denoted by asterisks ("*"), and "P", "T" and "N" denote the ones with scores from 95% to 99%. Poles of nodal planes are shown by "A" and "B": Open and solid circles denote dilatation and compression of first-motion, respectively. Numbers of observed first-motion data are given by N. For saving the space the presentation is made for only the earthquakes mentioned in the text.

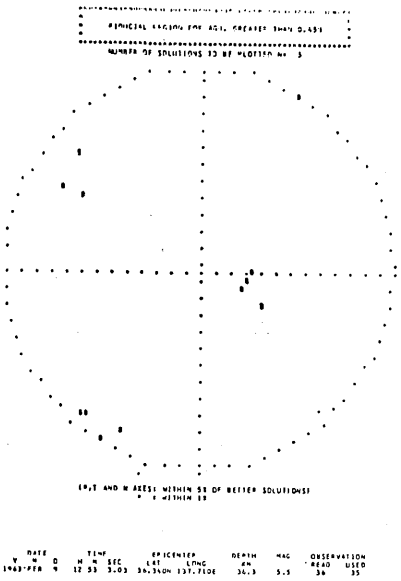

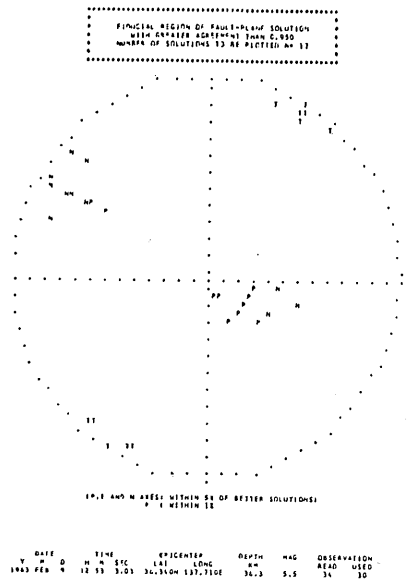

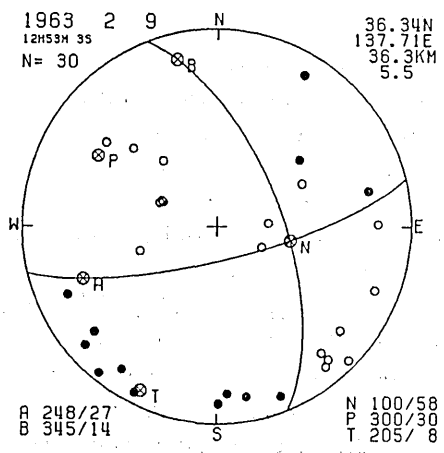
1963 2 9
12H53M 3S
N= 30
36.3N
137.7E
36.3KM
5.5
N
W
E
S
P
B
N
H
T
A 248/27
B 345/14
N 100/58
P 300/30
T 205/ 8

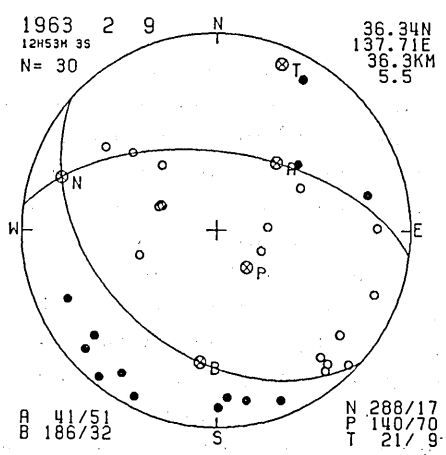
1963 2 9
12H53M 3S
N= 30
36.3N
137.7E
36.3KM
5.5
N
W
E
S
T
N
H
P
B
A 41/51
B 186/32
N 288/17
P 140/70
T 21/ 9

A 1

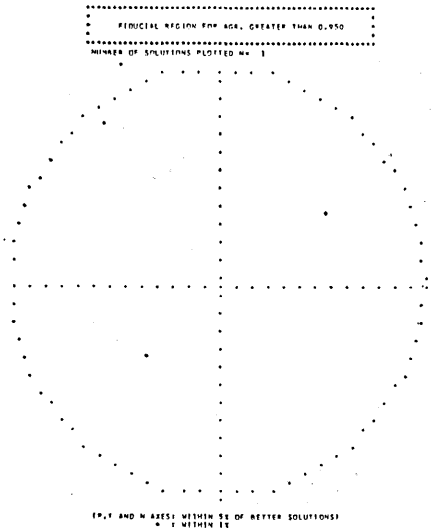

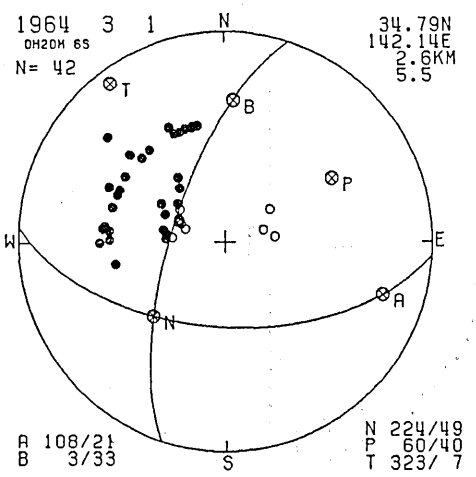

DATE Y	M	D	TIME H	M	SEC	EPICENTER LAT	LONG	DEPTH KM	MAG	OBSERVATION READ	USED
1964	MAR	1	0	20	0.21	34.79ON	142.14OE	2.6	5.5	95	0

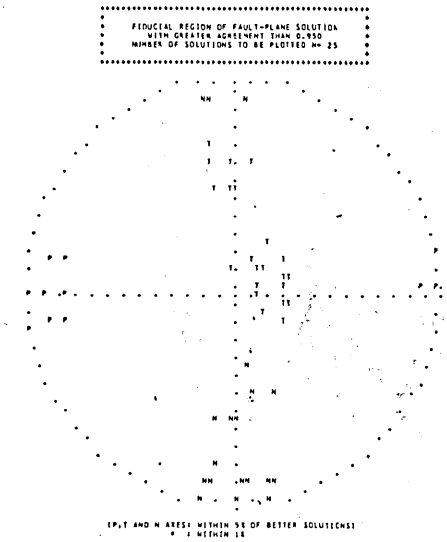

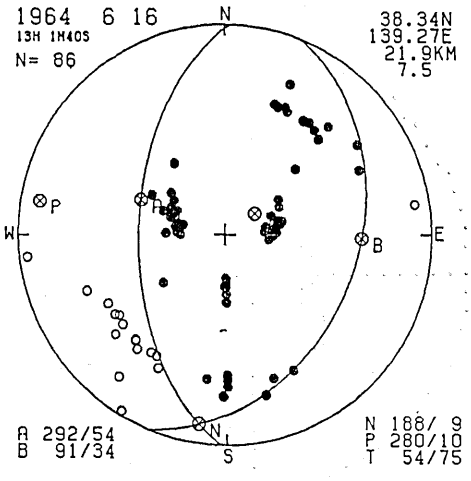

DATE Y	M	D	TIME H	M	SEC	EPICENTER LAT	LONG	DEPTH KM	MAG	OBSERVATION READ	USED
1964	JUN	16	13	1	40.61	38.34ON	139.27OE	21.9	7.5	96	86

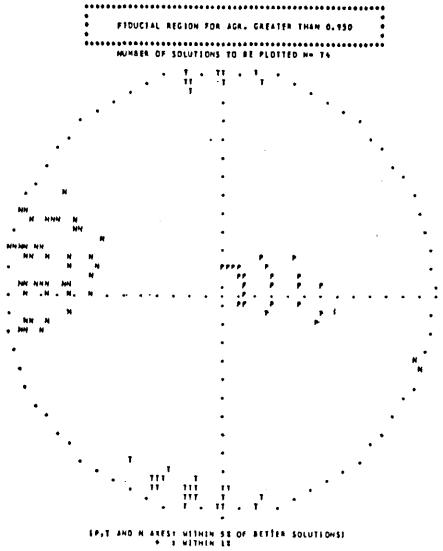

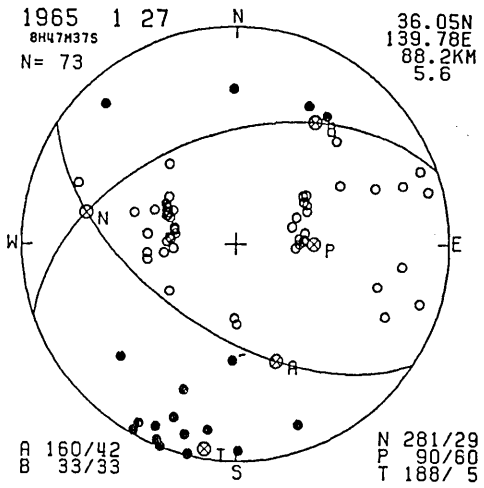

DATE Y M D	TIME H M SEC	EPICENTER LAT	LONG	DEPTH KM	MAG	OBSERVATION READ	USED
1965 JAN 27	8 47 37.01	36.05ON	139.78OE	88.2	5.6	87	73

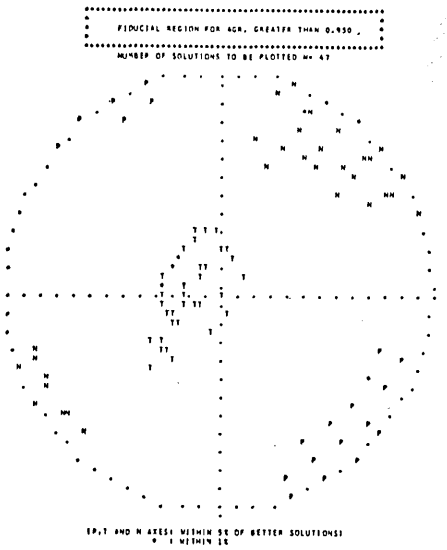

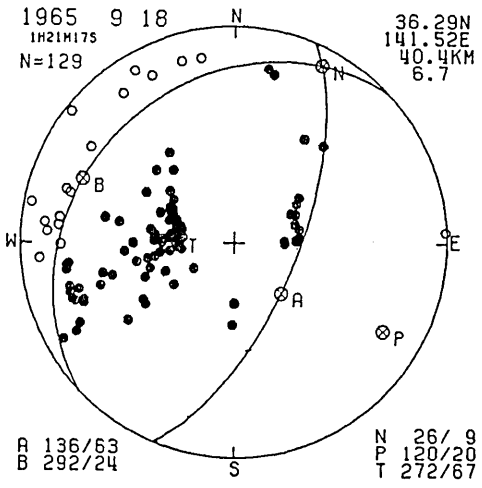

DATE Y M D	TIME H M SEC	EPICENTER LAT	LONG	DEPTH KM	MAG	OBSERVATION READ	USED
1965 SEP 18	1 21 17.97	36.29ON	141.52OE	40.4	6.7*	137	129

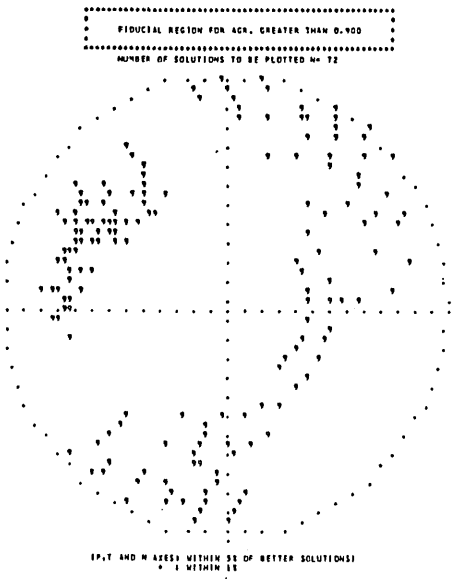

DATE Y	M	D	TIME H	M	SEC	EPICENTER LAT	LONG	DEPTH KM	MAG	OBSERVATION READ	USED
1966 APR	22		0	45	22.35	35.61ON	142.08OE	52.0	5.8	48	43

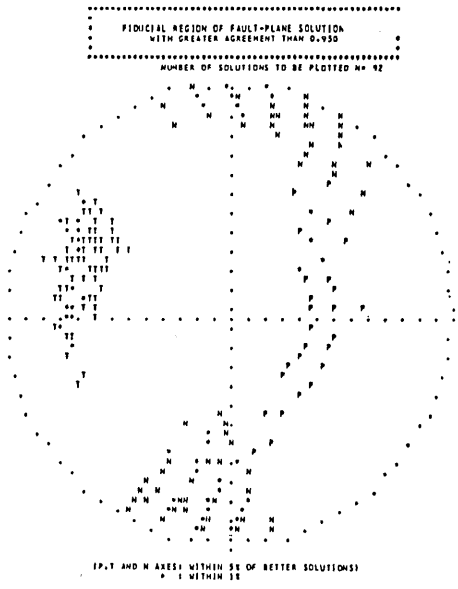

DATE Y	M	D	TIME H	M	SEC	EPICENTER LAT	LONG	DEPTH KM	MAG	OBSERVATION READ	USED
1966 APR	22		0	45	22.35	35.61ON	142.08OE	52.0	5.8	43	39

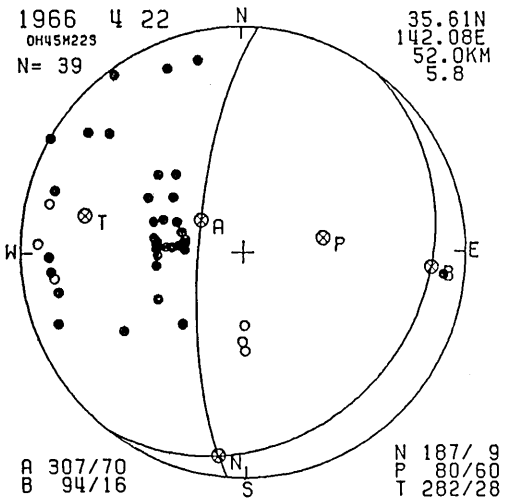

A 4

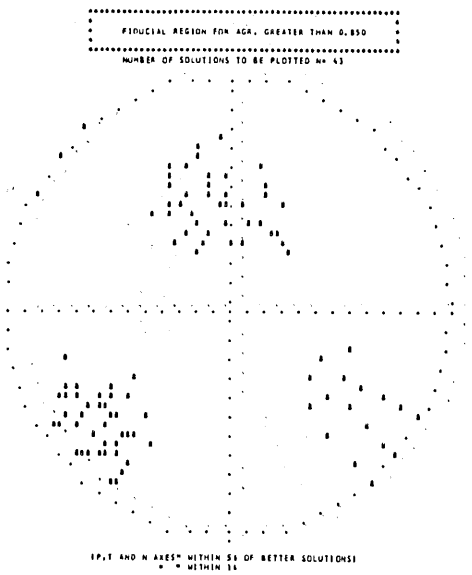

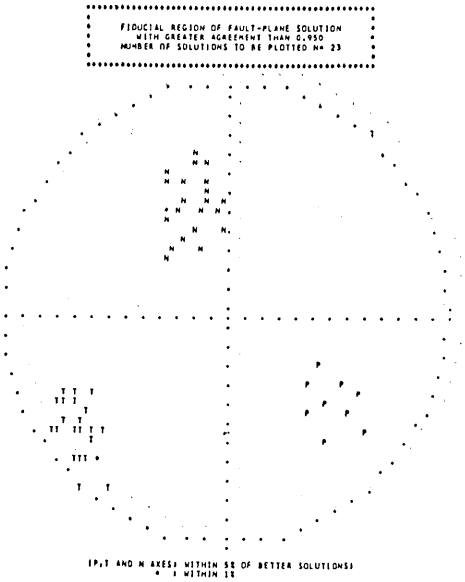

DATE Y M D	TIME H M SEC	EPICENTER LAT	LONG	DEPTH KM	MAG	OBSERVATION READ	USED
1967 MAR 19	2 49 48.71	36.28ON	140.05OE	97.3	5.5	74	67

DATE Y M D	TIME H M SEC	EPICENTER LAT	LONG	DEPTH KM	MAG	OBSERVATION READ	USED
1967 MAR 19	2 49 48.71	36.28ON	140.05OE	97.3	5.5	47	58

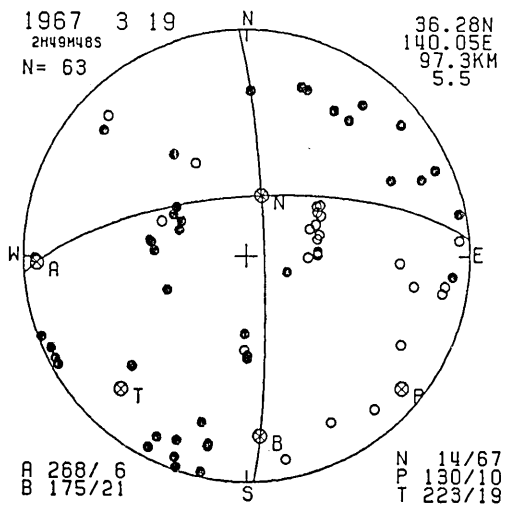

A 5

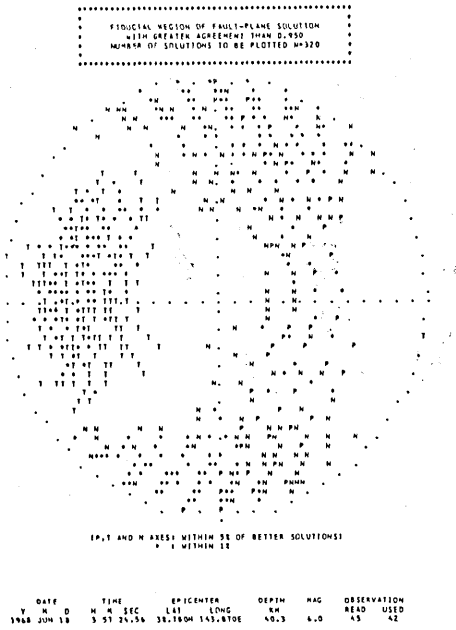
FIDUCIAL REGION OF FAULT-PLANE SOLUTION
WITH GREATER AGREEMENT THAN 0.950
NUMBER OF SOLUTIONS TO BE PLOTTED M=320
(P,T AND N AXES WITHIN 55 OF BETTER SOLUTIONS)
WITHIN 15
DATE
TIME
EPICENTER
DEPTH
MAG
OBSERVATION
Y M D
H M SEC
LAT
LONG
KM
READ
USED
1968 JUN 18
5 57 31.56
38.78ON 143.87OE
40.3
6.0
43
42

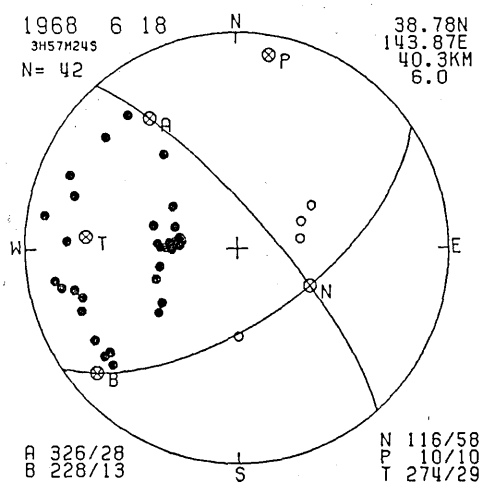
1968 6 18
3H57M24S
N= 42
38.78N
143.87E
40.3KM
6.0
N
P
A
W
T
E
N
B
S
A 326/28
B 228/13
N 116/58
P 10/10
T 274/29

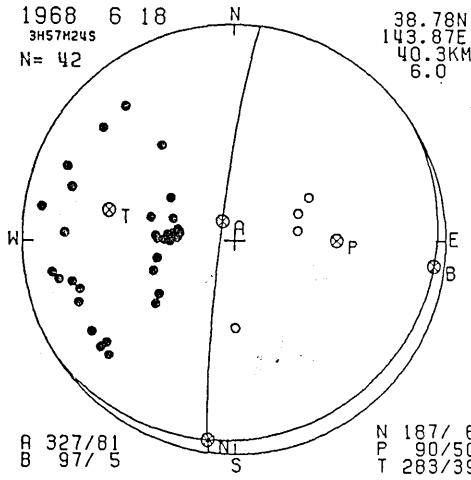
1968 6 18
3H57M24S
N= 42
38.78N
143.87E
40.3KM
6.0
N
W
T
A
P
E
B
N
S
A 327/81
B 97/ 5
N 187/ 6
P 90/50
T 283/39

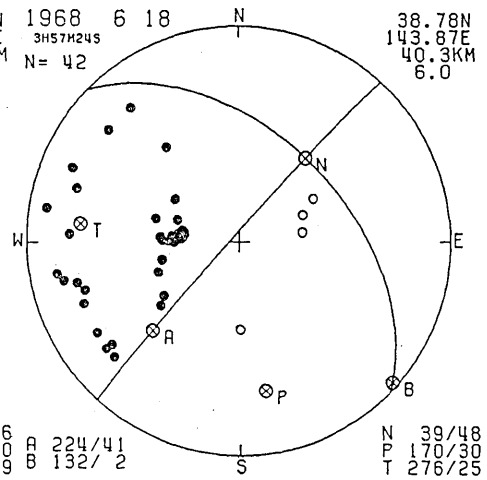
1968 6 18
3H57M24S
N= 42
38.78N
143.87E
40.3KM
6.0
N
W
T
E
N
A
P
B
S
A 224/41
B 132/ 2
N 39/48
P 170/30
T 276/25

A 6

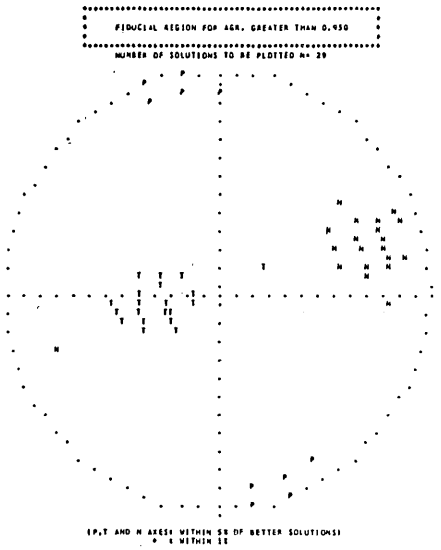

DATE Y	M	D	TIME H	M	SEC	EPICENTER LAT	LONG	DEPTH KM	MAG	OBSERVATION READ	USED
1968	JUL	1	19	45	12.13	35.97ON	139.38OE	60.8	6.1	196	175

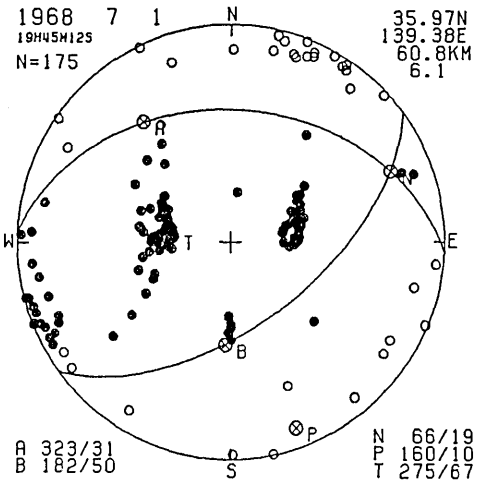

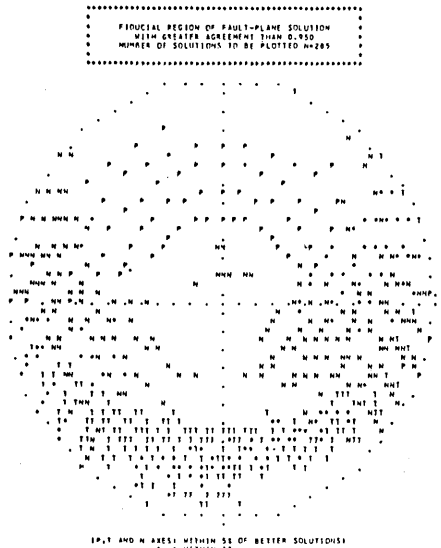

DATE Y	M	D	TIME H	M	SEC	EPICENTER LAT	LONG	DEPTH KM	MAG	OBSERVATION READ	USED
1968	OCT	29	13	6	6.56	31.56ON	141.97OE	16.3	5.4	77	61

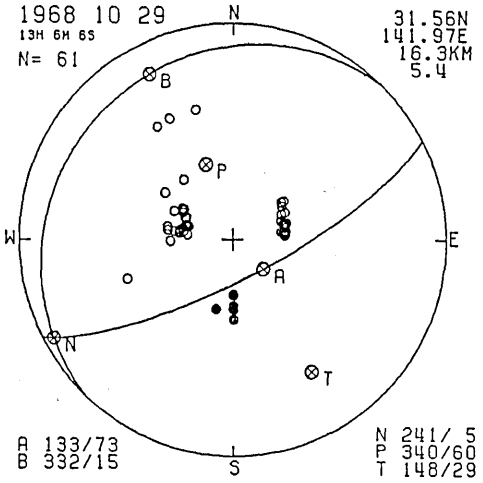

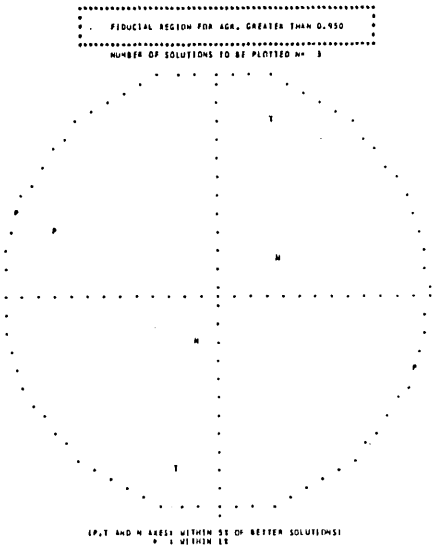

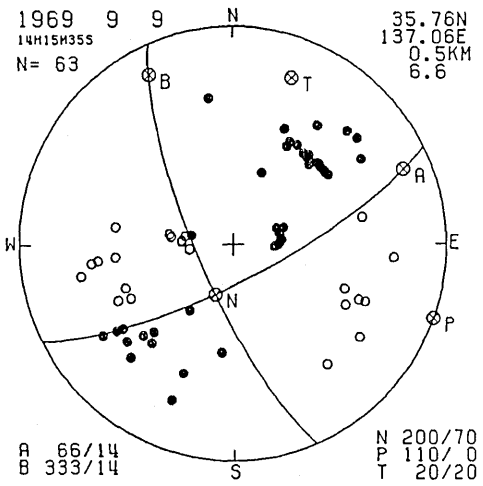

DATE Y M D	TIME H M SEC	EPICENTER LAT	LONG	DEPTH KM	MAG	OBSERVATION READ	USED
1969 SEP. 9	14 15 35.54	35.76ON	137.06OE	0.5	6.6	105	63

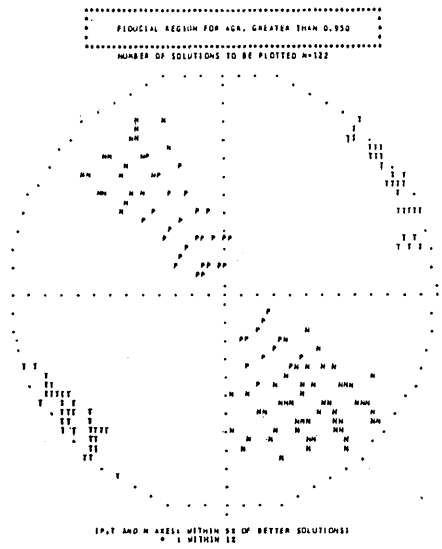

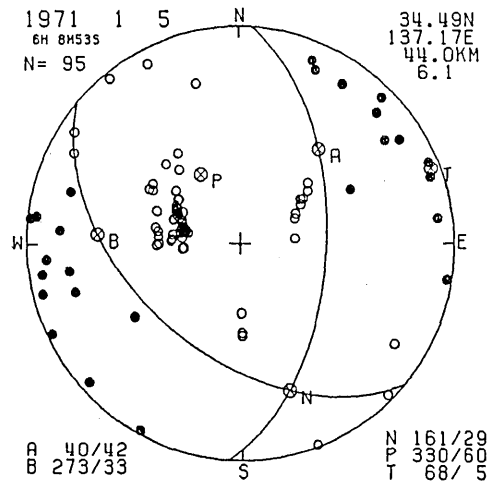

DATE Y M D	TIME H M SEC	EPICENTER LAT	LONG	DEPTH KM	MAG	OBSERVATION READ	USED
1971 JAN 5	6 8 53.05	34.49ON	137.17OE	44.0	6.1	121	95

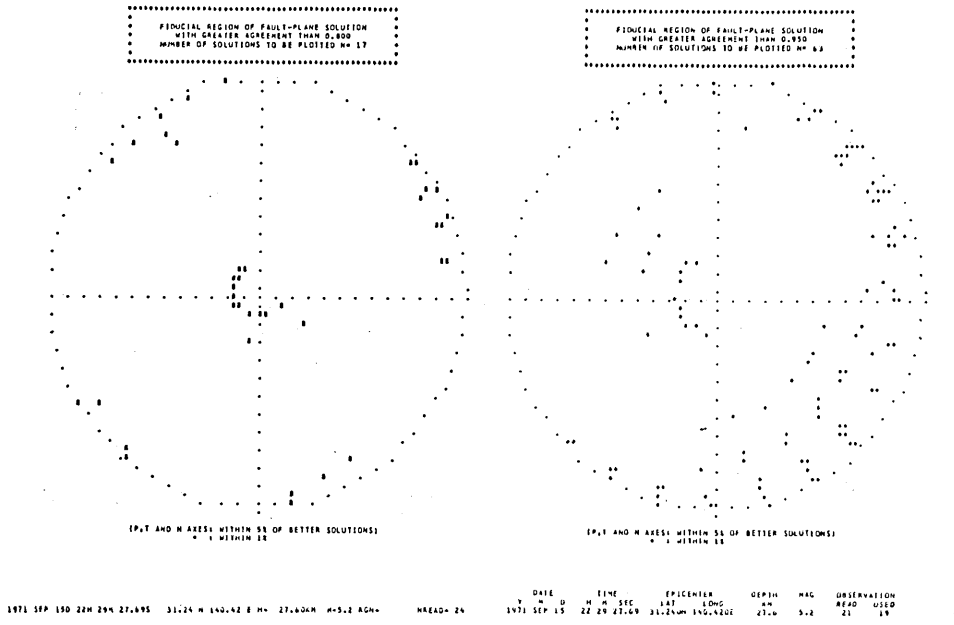
FIDUCIAL REGION OF FAULT-PLANE SOLUTION
WITH GREATER AGREEMENT THAN 0.800
NUMBER OF SOLUTIONS TO BE PLOTTED N= 17
(P,T AND N AXES WITHIN 55 OF BETTER SOLUTIONS)
FIDUCIAL REGION OF FAULT-PLANE SOLUTION
WITH GREATER AGREEMENT THAN 0.950
(P,T AND N AXES WITHIN 55 OF BETTER SOLUTIONS)
DATE
TIME
EPICENTER
DEPTH
MAG
OBSERVATION
1971 SEP 15
22 29 27.69
31.24N
140.42E
27.6
5.2

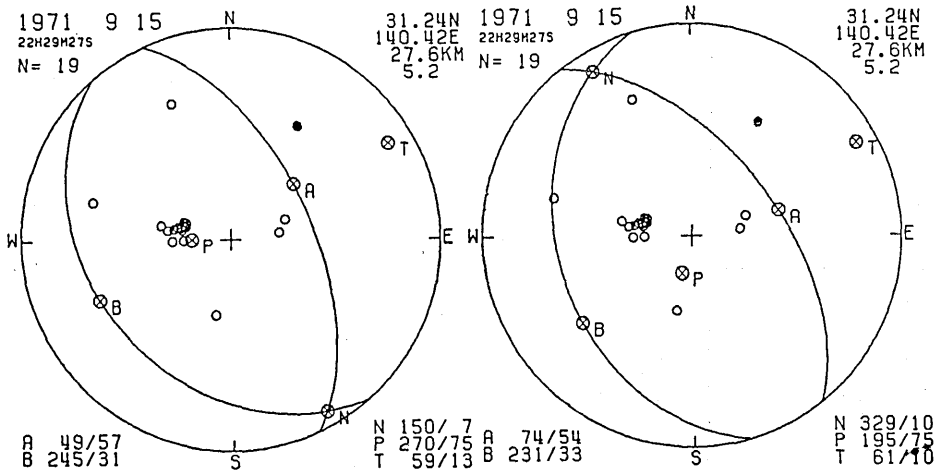
1971 9 15
22H29M27S
N= 19
31.24N
140.42E
27.6KM
5.2
N
W
E
S
T
A
B
P
N
A 49/57
B 245/31
N 150/ 7
P 270/75
T 59/13
1971 9 15
22H29M27S
N= 19
31.24N
140.42E
27.6KM
5.2
A 74/54
B 231/33
N 329/10
P 195/75
T 61/10

A 9

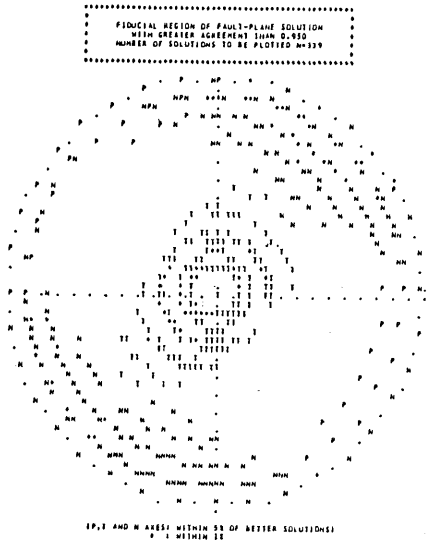

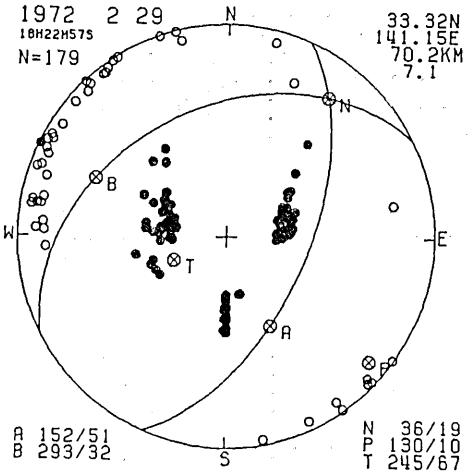

DATE Y M D	TIME H M SEC	EPICENTER LAT	LONG	DEPTH KM	MAG	OBSERVATION READ	USED
1972 FEB 29	18 22 57.88	33.32ON	141.15OE	70.2	7.1	204	179

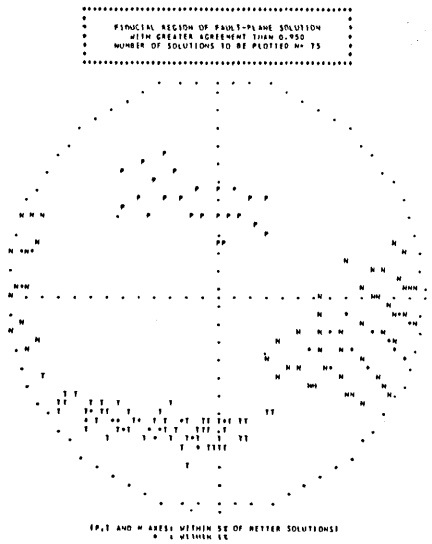

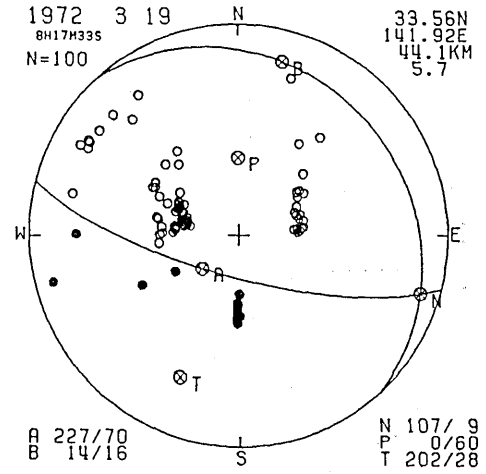

DATE Y M D	TIME H M SEC	EPICENTER LAT	LONG	DEPTH KM	MAG	OBSERVATION READ	USED
1972 MAR 19	8 17 33.61	33.56ON	141.92OE	44.1	5.7	131	100

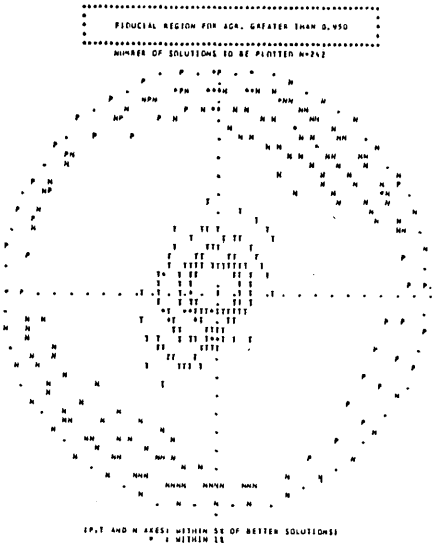

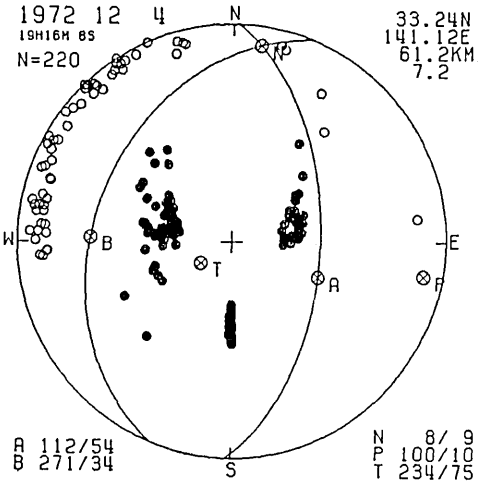

DATE Y	M	D	TIME H	M	SEC	EPICENTER LAT	LONG	DEPTH KM	MAG	OBSERVATION READ	USED
1972	DEC	4	19	16	8.83	33.24ON	141.12OE	61.2	7.2	254	220

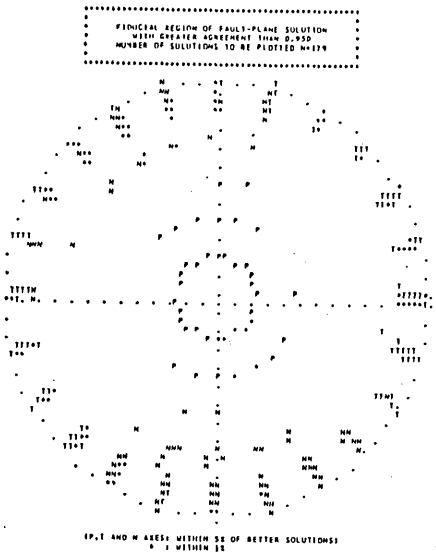

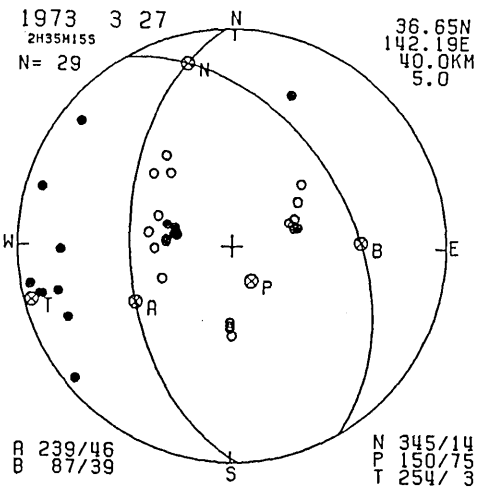

DATE Y	M	D	TIME H	M	SEC	EPICENTER LAT	LONG	DEPTH KM	MAG	OBSERVATION READ	USED
1973	MAR	27	2	35	15.3s	36.65ON	142.19OE	40.0	5.0	35	29

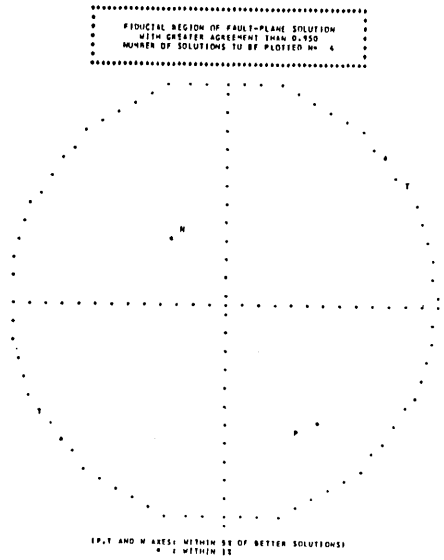

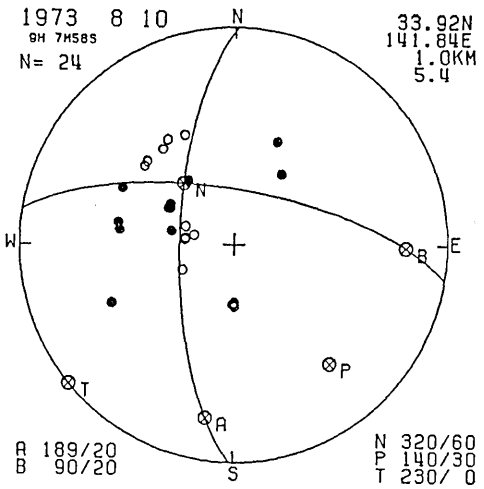

DATE Y	M	D	TIME H	M	SEC	EPICENTER LAT	LONG	DEPTH KM	MAG	OBSERVATION READ	USED
1973	AUG	10	9	7	58.32	33.92ON	141.84OE	1.0	5.4	34	24

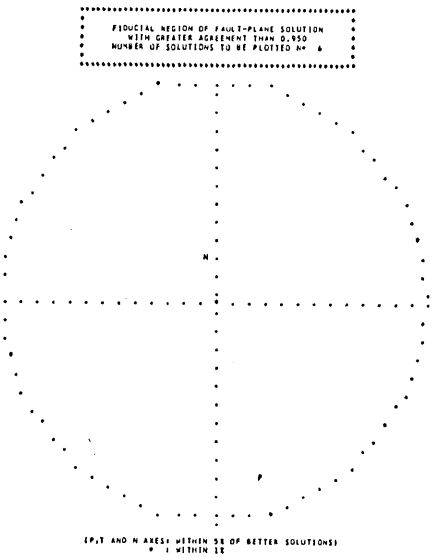

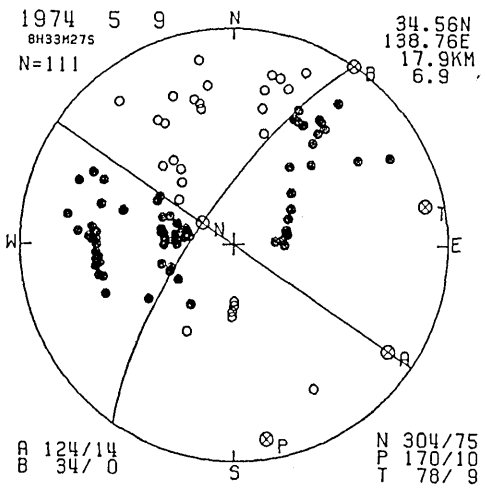

DATE Y	M	D	TIME H	M	SEC	EPICENTER LAT	LONG	DEPTH KM	MAG	OBSERVATION READ	USED
1974	MAY	9	8	33	27.22	34.56ON	138.76OE	17.9	6.9	134	101

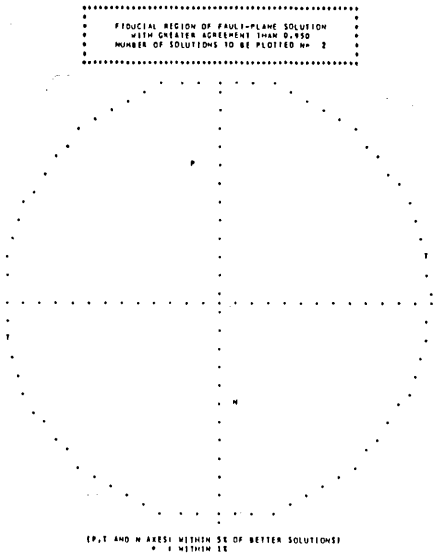

DATE Y	M	D	TIME H	M	SEC	EPICENTER LAT	LONG	DEPTH KM	MAG	OBSERVATION READ	USED
1974	JUN	27	10	49	9.2E	33.69DN	139.29DE	49.8	6.1	79	60

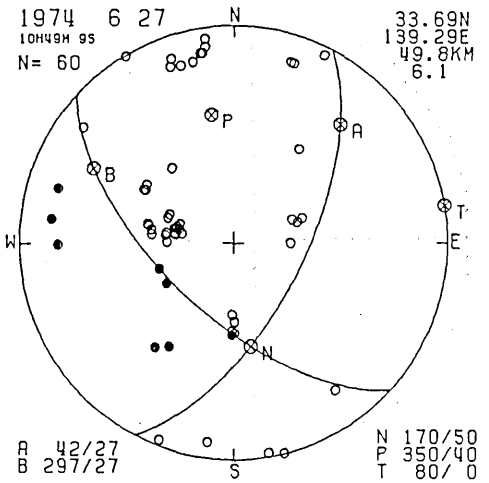

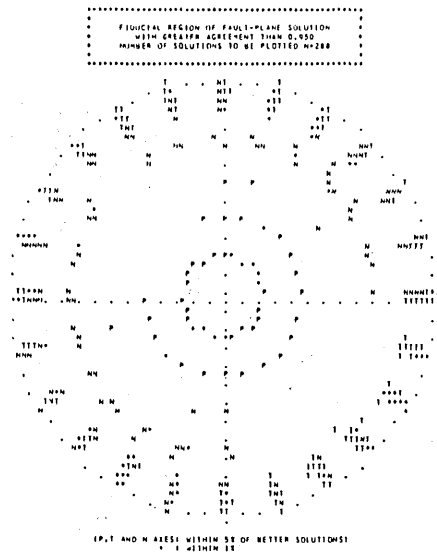

DATE Y	M	D	TIME H	M	SEC	EPICENTER LAT	LONG	DEPTH KM	MAG	OBSERVATION READ	USED
1974	AUG	25	10	18	36.7E	32.08DN	142.79DE	44.0	5.8	135	135

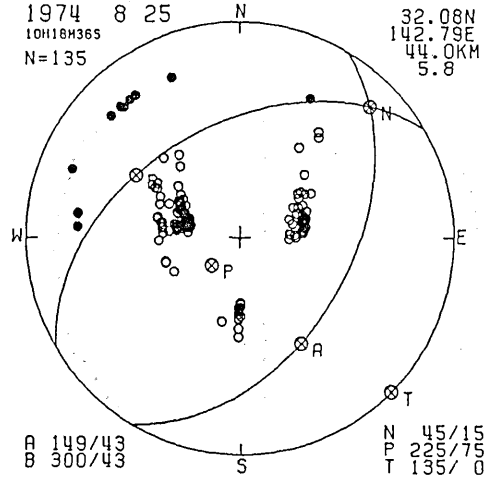

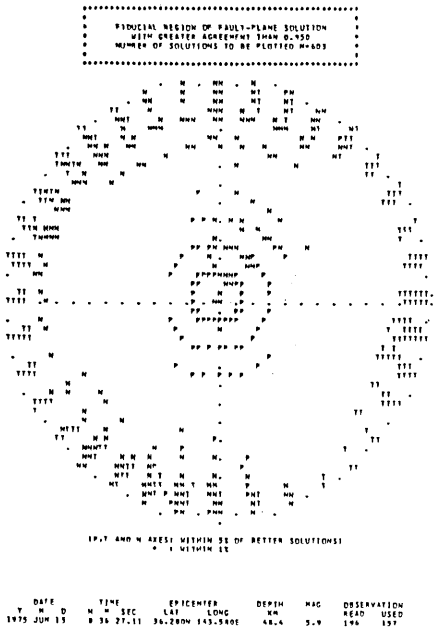

DATE Y	M	D	TIME H	M	SEC	EPICENTER LAT	LONG	DEPTH KM	MAG	OBSERVATION READ	USED
1975 JUN 15			8	36	27.11	36.28ON	143.58OE	48.4	5.9	196	157

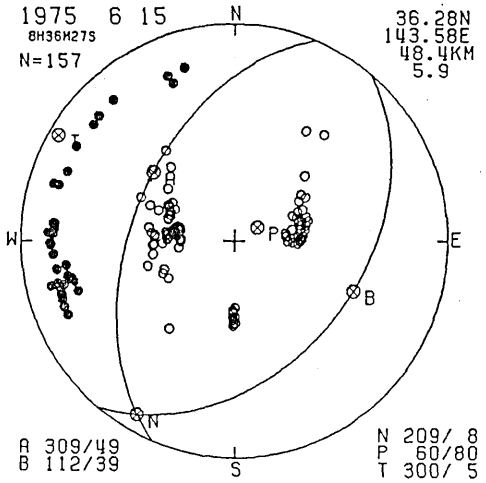

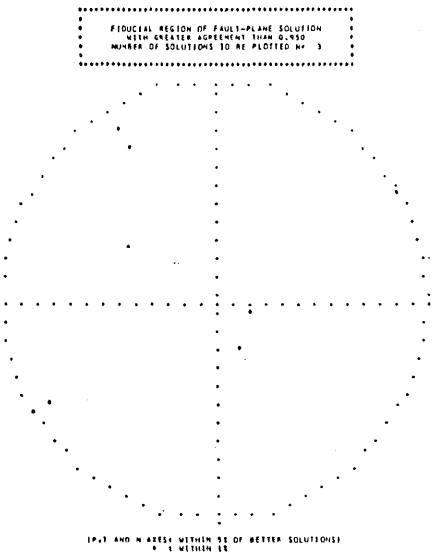

DATE Y	M	D	TIME H	M	SEC	EPICENTER LAT	LONG	DEPTH KM	MAG	OBSERVATION READ	USED
1978 JAN 14			12	24	38.60	34.72ON	139.31OE	20.7	7.0	150	94

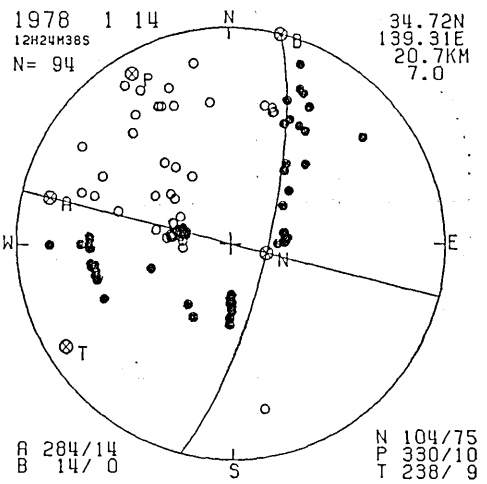

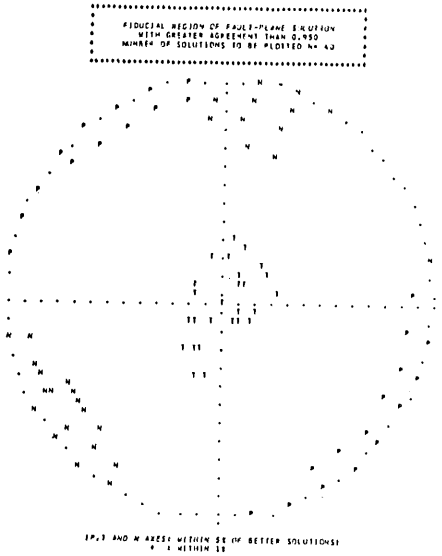

DATE Y	M	D	TIME H	M	SEC	EPICENTER LAT	LONG	DEPTH KM	MAG	OBSERVATION READ	USED
1978	JUN	12	17	14	26.26	38.190N	142.140E	32.2	7.4	248	221

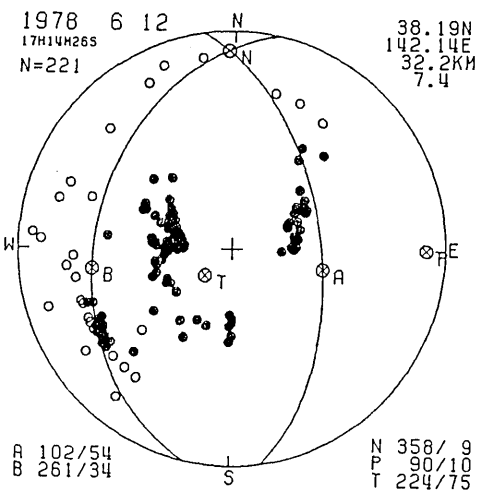

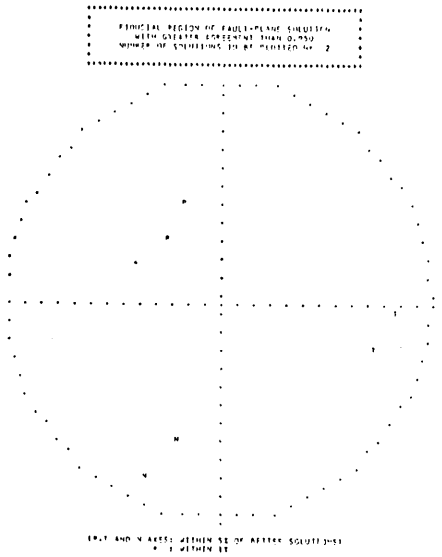

DATE Y	M	D	TIME H	M	SEC	EPICENTER LAT	LONG	DEPTH KM	MAG	OBSERVATION READ	USED
1979	AUG	12	16	13	19.43	34.590N	140.440E	53.0	5.7	144	123